REVIEW ARTICLE

Check for updates

Advancements and opportunities in piezo-(photo)-catalytic synthesis of value-added chemicals

Weiliang Qi, [ID] †[a] Yaping Fu,†[a] Enbo Liu,[a] Zhixing Cheng, [ID] [b] Yuxiu Sun,[a] Siqi Liu [ID] [a] and Minghui Yang [ID] *[a]

Piezo-(photo)catalytic technologies offer a promising solution for accelerating energy diversification and addressing environmental pollution by converting mechanical and light energy into chemical energy. The application of piezo-(photo)catalytic technology not only meets the demands of a growing market but also contributes to environmental preservation. In this review, we summarize recent advancements in synthesizing value-added chemicals through piezo-(photo)catalytic technology, highlighting the principles of piezotronics and piezo-phototronics. We examine the fundamental processes involved in energy conversion and discuss the advantages of synthesized value-added chemicals using piezocatalytic technology. We explore different chemistries and reaction pathways, and categorize piezoelectric semiconductors based on performance in piezo-photocatalysis. Finally, we identify prospects, challenges, and potential solutions for future research and development in value-added chemical synthesis using piezo-(photo)catalytic technology.

Broader context

The challenges of energy shortages and environmental pollution have compelled people to address these difficulties by exploring and harnessing a variety of renewable energy sources. Piezocatalysis and piezo-photocatalysis technologies offer a viable pathway to accelerate the diversification of energy supply and address environmental pollution issues by converting renewable energy (mechanical and light energy) into chemical energy. Catalysts with non-centrosymmetric structures can continuously facilitate or promote the occurrence of chemical reactions under the influence of sustained external mechanical forces. Utilizing piezo-(photo)catalytic technology for the value-added synthesis of chemicals offers a mild, green process with few byproducts. Simultaneously, compared to traditional methods of chemical synthesis, piezo-(photo)catalytic technology typically has lower energy consumption and carbon emissions. It can meet the ever-increasing market demand for chemicals while simultaneously considering environmental protection. However, currently, there are no available studies that comprehensively summarize and introduce the current state of piezo-(photo)catalytic technology for the synthesis of value-added chemicals. This article primarily reviews the recent advances in the application of piezocatalytic and piezo-photocatalytic technologies in the value-added synthesis of chemicals, with the aim of contributing to the production of value-added chemicals and the design of efficient piezo-photocatalytic systems.

1. Introduction

Rapid growth of the global population and unprecedented industrial development have forced people to confront the challenges of energy shortages and environmental pollution.[1] Scientists across multiple disciplinary fields are working tirelessly to overcome these predicaments by engaging in the development and utilization of various renewable energy sources.[2,3] Effectively harnessing and converting renewable energy from natural sources such as sunlight, vibration, friction, natural wind, and tidal forces into chemical energy can significantly alleviate the current challenges related to energy and environmental issues.[4,5] With the proposal and development of the piezoelectric effect, technologies based on piezocatalysis and piezo-photocatalysis, which utilize the piezoelectric effect and piezo-phototronic effect, are receiving increasing attention in the fields of renewable energy collection and catalytic chemistry.[6,7] Especially, piezo-(photo)catalytic materials that integrate the piezoelectric effect with photo/electrochemical reaction processes offer new ideas for multi-renewable energy synergistic collectors.[8]

Piezoelectric catalytic materials generally refer to a special class of crystalline materials with non-central symmetric

[a] *School of Environmental Science and Technology, Dalian University of Technology, Dalian 116024, P. R. China. E-mail: myang@dlut.edu.cn*

[b] *School of Fashion & Textiles, The Hong Kong Polytechnic University, Hong Kong 100872, P. R. China*

† These authors contributed equally.

structures.[9] They can respond to external mechanical energy, converting it into electrical energy, and subsequently intervene in chemical reactions on the material's surface to further transform it into chemical energy.[10] This mechano-electro-chemical energy conversion behavior originates from the anisotropy of the catalyst structure.[11] When the

piezocatalyst is subjected to external mechanical forces or undergoes strain, the displacement of atoms within the crystal cell causes the positive and negative charge centers to not coincide, resulting in the formation of a dipole moment (polarization).[11] After the dipole moments are arranged in an orderly manner, a macroscopic internal

Weiliang Qi is currently a Postdoc fellow at the Dalian University of Technology. He completed his PhD in Materials Physics and Chemistry under the supervision of Professor Minghui Yang at the Ningbo Institute of Materials Technology & Engineering, Chinese Academy of Sciences in 2023. His main research interests focus on the design and synthesis of transition metal nitride-based catalysts for heterogeneous photocatalysis and pizeocatalysis.

Weiliang Qi
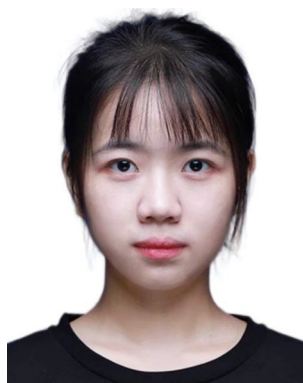
Yaping Fu is studying for a master's degree under the supervision of Prof. Minghui Yang at the Dalian University of Technology. Her main interest is the synthesis of transition metal nitrides and their use in heterogeneous photocatalysis and pizeocatalysis.

Yaping Fu

Enbo Liu is studying for a master's degree under the supervision of Prof. Minghui Yang at the Dalian University of Technology. His main interest is the synthesis of transition metal nitride-based catalysts for heterogeneous pizeocatalysis.

Enbo Liu

Zhixing Cheng is currently a Postdoc fellow at The Hong Kong Polytechnic University. He completed his PhD in Chemical Environmental Engineering under the supervision of Prof. Tao Wu at the University of Nottingham Ningbo China and Prof. Minghui Yang at the Ningbo Institute of Materials Technology & Engineering, Chinese Academy of Sciences in 2021. His main research interests focus on the fabrication of porous transition metal nitride-based and phosphide-based catalysts for heterogeneous photocatalysis.

Zhixing Cheng

Yuxiu Sun is studying for a master's degree under the supervision of Prof. Minghui Yang at the Dalian University of Technology. His main interest is the synthesis of Mxene-based catalysts and their use in pizeocatalytic hydrogen peroxide production.

Yuxiu Sun

Siqi Liu is an Associate research fellow at the Dalian University of Technology. He received PhD degree from Fuzhou University. His current research interests primarily focus on the synthesis and applications of transition metal nitride-based nanostructured composite photo-catalysts, in the field of heterogeneous photocatalysis.

Siqi Liu

electric field/potential field (polarization field/piezoelectric potential) is established.[12] By continuously applying external mechanical energy, the piezoelectric catalyst can facilitate sustained chemical reactions.[9]

Semiconductor photocatalysts with piezoelectric properties can utilize these piezoelectric potential and polarized charges to simultaneously collect and convert mechanical energy and solar energy.[7] This coupling effect between piezoelectric polarization and photoelectric processes, known as the piezo-phototronic effect, can provide the driving force for the transport of photogenerated electrons/holes.[13] The piezoelectric polarization charges and induced piezoelectric potential enable photogenerated charges in piezoelectric semiconductor photocatalysts to migrate in specific directions, promoting their separation and reducing their recombination.[14] This piezo-phototronic effect, which is based on the coupling of semiconductor properties, photoexcitation, and piezoelectric characteristics, offers new insights to some extent into addressing two key challenges in photocatalysis: the instability of solar light and the inefficient separation of carriers.[15] Particularly, the challenge of the instability of solar light, which hinders the scalability of photocatalytic applications, can be mitigated by the continuity of mechanical energy required in piezo-photocatalysis.

Based on piezotronics and piezo-phototronics, piezo-(photo)catalysis has seen rapid development over more than a decade since the groundbreaking works of Xu's and Wang's research group in 2010.[16,17] As of now, piezo-(photo)catalysis has garnered intense interest in multiple scientific fields such as physics, chemistry, energy, and environmental science,[18–20] and piezo-(photo)catalytic materials have been applied in hydrogen production, carbon dioxide reduction, organic synthesis, biological applications, environmental remediation, and small molecule catalysis.[21–24] As research on piezotronics and piezo-phototronics continues to deepen, researchers' understanding of piezo-(photo)catalysis is also constantly being updated and experiencing breakthroughs. To date, several review articles related to piezoelectric (photo)catalysis have been published. Regarding the piezoelectric mechanism, Liu et al. have comprehensively summarized and explained two distinguishable theories of piezocatalysis: the energy band theory and the screening charge effect.[12] Tudela et al. have summarized the fundamental knowledge of piezocatalysis from different perspectives, including piezoelectric, electrochemical, and sonochemical aspects.[25] Wang et al. have elucidated the mechanism of piezo-photocatalysis from the perspective of enhancement effects of the piezo-phototronic effect.[26] From the perspective of the design and modification of piezoelectric materials, Huang et al. have provided a comprehensive summary of the design strategies for efficient piezocatalytic systems.[27] Yan et al. starting from the intersection of solid-state physics and catalytic chemistry, have summarized the design strategies for piezocatalytic systems.[9] From an application perspective, our research group has recently provided a detailed summary of the research progress in piezocatalysis in the field of environmental remediation.[28] Shi et al. have summarized the research progress of piezocatalysis in medicine in aspects such as tissue repair and regeneration, tumor treatment, and biosensing.[29] Sudrajat et al. discussed the prospects and challenges of piezocatalytic CO2 reduction.[30] Despite these excellent reviews summarizing the work in the field of piezo-(photo)catalysis, we have noticed that there is still a lack of comprehensive summaries in the area of synthesizing value-added chemicals through piezo-(photo)catalysis, a research hotspot that has garnered increasing interest in recent years. Particularly considering that piezo-(photo)catalysis technology, which can collect mechanical (as well as solar) energy, is used for the production of high-value chemicals, it is extremely valuable for the future development of energy and environmental science. Therefore, a comprehensive and systematic summary focusing on the synthesis of value-added chemicals through piezo-(photo)catalysis is highly anticipated and urgently needed.

Herein, we comprehensively summarize the current progress in the synthesis of value-added chemicals through piezo-(photo)catalysis. At first, the mechanisms of piezocatalysis and piezo-photocatalysis are introduced from the perspectives of piezoelectric materials, piezo-(photo)tronics, and catalytic chemistry. Then, the advancements in synthesizing different value-added chemicals through piezocatalysis are introduced, with a detailed summary of the performance and catalytic mechanisms of various catalytic materials in synthesizing different value-added chemicals. Subsequently, categorizing by piezoelectric semiconductors, the latest developments in the synthesis of value-added chemicals through piezo-photocatalysis are summarized. Finally, a detailed summary and outlook are provided on the prospects and challenges of synthesizing chemicals *via* piezo-(photo)catalysis, offering new insights and directions for the field of piezo-(photo)catalysis and the synthesis of value-added chemicals.

Minghui Yang is a Professor at the Dalian University of Technology. He received M.Chem. degree from the University of Liverpool and completed his PhD in Materials Chemistry under the supervision of Prof. J. Paul Attfield at the University of Edinburgh. This was followed by a postdoctoral appointment in the Department of Chemistry and Chemical Biology at Cornell University, where he worked on nano-structured metal nitrides with Francis J. DiSalvo.

Minghui Yang

He has more than 200 publications to his credit including those in Nature Materials, Nature Chemistry, etc. His current research is centered on solid state functional materials for catalysis and sensing applications.

2. The fundamentals and principles of piezocatalysis and piezo-photocatalysis

2.1 Piezocatalysts and piezo-photocatalyst

Piezocatalysts refer to those materials with piezoelectric properties that can collect mechanical energy to initiate various redox reactions. Their development began with the discovery of piezoelectric natural single crystals α-quartz and Rochelle salt ($NaKC_4H_4O_6·4H_2O$).[9] Due to the limitations of the piezoelectric effect, catalysts lacking piezoelectric properties cannot respond to mechanical energy even when sufficient strain is applied. The piezoelectric characteristics of piezocatalysts originate from their non-centrosymmetric structure.[31] Therefore, among the 32 different crystal point groups in the seven crystal systems, 11 centrosymmetric crystals cannot act as piezocatalysts, while among the 21 non-centrosymmetric crystals, 20 have been confirmed to serve as piezocatalysts (the 432 point group has relatively lower asymmetry).[27,28] As of now, materials such as chalcogenides, perovskites, layered bismuth-based materials, layered structure two-dimensional materials, and piezoelectric polymers have been used as piezocatalysts in a variety of different piezocatalytic reactions.[28,32,33] Simultaneously, seeking effective ways to disrupt the symmetry of materials to endow non-typical piezoelectric materials with piezoelectric properties is gradually becoming an important research topic, thereby continuously increasing the variety of piezocatalysts. These novel piezocatalysts continually breathe new life into the field of piezocatalysis.

In addition to the intrinsic piezoelectricity of the piezocatalysts, the mechanical energy that induces strain, as well as the thickness in the direction of the electric dipoles of the piezocatalysts also play a crucial role in piezocatalysis.[10,27] It is well known that the strain in piezocatalysts is indispensable for initiating piezocatalytic reactions. Therefore, to ensure the sustainability of chemical reactions, it is essential to maintain the periodicity of the strain. Currently, mechanical vibrations such as the bursting pressure of cavitation bubbles, ultrasonic vibrations from ultrasound, water flow providing shear force, ball milling, and thermal stress can all provide sustainable cyclic stress for piezocatalysis.[34,35] This greatly ensures the wide application of piezocatalysis. The thickness of the piezocatalyst in the direction of the electric dipoles is directly proportional to the piezoelectric potential. The piezocatalytic reaction can occur only when the piezoelectric potential provided by the piezocatalyst is sufficient.[36] Of course, the efficiency of piezocatalysts is influenced not only by the piezoelectric properties of the materials, but also significantly affected by factors such as active sites on the catalyst surface, charge separation and diffusion, and surface reactions.[9] This also makes the modification of piezocatalysts a new research direction in the field of piezoelectricity.

For piezo-photocatalysts, their primary composition mainly comes from piezoelectric semiconductors. Traditional non-piezoelectric semiconductors are significantly constrained in photocatalytic reactions in terms of carrier recombination and transport efficiency.[37,38] By utilizing semiconductor materials with piezoelectric properties driven by mechanical energy, the piezoelectric effect and piezo-phototronic effect can be generated through piezoelectric polarization, thereby modulating the slow charge transfer process.[26] The tri-directional coupling between piezoelectric polarization, photon excitation, and charge transfer in semiconductors controls the redox catalytic performance of piezo-photocatalysts. In summary, piezo-photocatalysts based on piezotronics and piezo-phototronics generally produce two typical effects under external mechanical (or thermal) stimuli: (i) creating an internal electric field to control the migration and separation of carriers in the space charge region. (ii) Affecting the redox kinetics on the surface of piezo-photocatalysts.[13,17]

2.2 The mechanism of piezocatalysis

Although the mechanism of piezocatalysis originates from the piezoelectric effect and the theory of piezotronics, to date, two distinct mechanisms have evolved in piezocatalysis: the energy band theory and the screening charge effect.[12] Unlike the mechanisms of photocatalysis or electrocatalysis, which are almost universally recognized, these two different mechanisms of piezocatalysis have been acknowledged in a variety of research works. Although the two piezocatalytic mechanisms differ significantly, both are based on the theory of piezotronics, meaning that the piezoelectric potential plays a key role in both mechanisms of piezocatalysis. For the energy band theory, the magnitude of the piezoelectric potential significantly determines the degree of energy band bending, thereby regulating the redox capability of the catalyst (by adjusting the energy band structure). For the screening charge effect, the focus is mainly on the role of external screening charges in piezocatalytic reactions. In this mechanism, the piezoelectric potential directly determines whether the catalyst can undergo a chemical reaction. The piezoelectric potential must be equal to or greater than the Gibbs free energy change of the reaction to drive the occurrence of the piezocatalytic reaction. Subsequently, a detailed introduction to both mechanisms will be provided in this section.

The energy band theory is derived from the mature mechanism of photocatalytic energy bands and has evolved into this mechanism after combining with the theory of piezotronics. Similar to the photoexcitation process in semiconductors, in the energy band theory, piezocatalysts are excited by external mechanical stress (or the thermal effects caused by mechanical forces), thereby generating carriers. Simultaneously, changes in the polarization state adjust the energy band structure of the piezocatalyst, further enhancing its redox capability.[39] Specifically, under the influence of stress, the piezocatalyst generates a piezoelectric potential, thereby establishing an internal electric field. This field alters the energy of the carriers, and the bulk electronic states are affected, leading to the bending of the energy bands. As illustrated in Fig. 1a, initially, due to the mismatch in the energy band structure, the piezoelectric material is thermodynamically unfavorable for redox reactions. However, when the piezoelectric material is subjected to
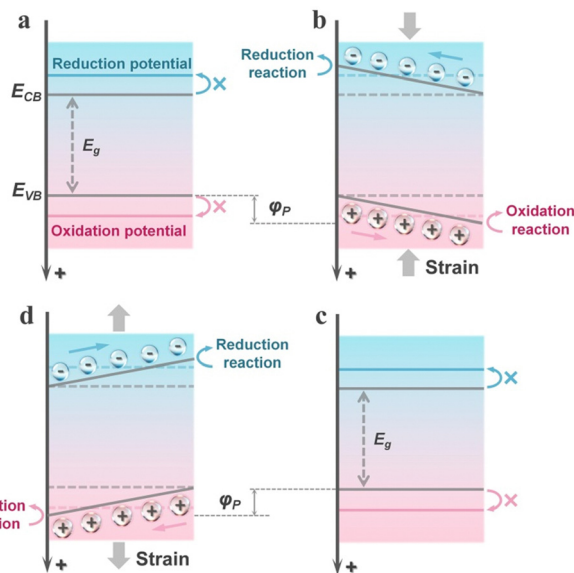
Fig. 1 Schematic illustration of the energy band theory of piezocatalytic mechanism, E_g and φ_P are the energy band gap and piezopotential, respectively. (a) Initial state. (b) Under compressive stress. (c) Return to initial state. (d) Under tensile stress.

external stress, the presence of the piezoelectric potential causes a significant bending of the energy bands, thereby shifting the band positions towards the potentials of redox reactions (Fig. 1b). For an actual piezocatalyst, when subjected to unidirectional stress, it results in the continuous accumulation of opposite moving charges on both polar sides under the influence of the piezoelectric potential. This generates a depolarization field, leading to the cancellation of the piezoelectric polarization effect and thereby shielding the bending of the energy bands (Fig. 1c). When the piezocatalyst is subjected to stress from another direction, this shielding effect is disrupted, resulting in a similar bending of the energy bands in the opposite direction (Fig. 1d). Therefore, this also explains why periodic stress can provide a continuous piezocatalytic reaction. The alternation of the piezoelectric potential field keeps the internal moving charges in a metastable state, rather than allowing them to accumulate in a directional manner. This can prevent the shielding of energy band bending and allows for the regulation of electronic energy levels in piezoelectric semiconductors. This is also the reason why ultrasonic waves are most commonly used to drive piezocatalytic reactions in current piezocatalysis research.[40] It is worth noting that the duration of strain maintained on the piezocatalyst in each individual strain cycle also has a very significant impact on the piezocatalytic activity. If the interval between two strain cycles is insufficient, the excited charges on the surface cannot exert their full effect, leading to a reduction in yield.[41] Therefore, when driving piezocatalytic reactions with ultrasonic waves or other alternating stresses, it is essential to achieve an optimal balance between strain frequency and the duration of each strain cycle to drive the piezocatalytic process as effectively as possible.

Different from the energy band theory, the screening charge effect posits that surface screening charges on the piezocatalyst play a key role in the piezocatalytic process, rather than the internal carriers. By regulating the polarization field through the piezoelectric effect, it is possible to precisely control the dynamic adsorption and desorption behavior of screening charges.[42] Here, the screening charge effect is introduced using the generation of reactive oxygen species (ROS) by the piezocatalyst as an example. In the initial state, the piezocatalyst is electrically neutral (Fig. 2a), as the bound charges caused by polarization are balanced by external screening charges, presenting opposite states on the two polar surfaces. Under the action of externally applied compressive stress, the charge balance state is disrupted, and the polarization is weakened, resulting in the release of additional screening charges from the surface (Fig. 2b). These free charges with sufficient energy undergo redox reactions with reactants near the surface of the catalyst (generating ROS). This stage continues with the ongoing changes in the screening charges, until a new electrostatic equilibrium is reached (Fig. 2c). As the external stress is removed, the polarization state is restored, leading to the generation of more polarization-bound charges. This results in the space charges from the electrolyte being reabsorbed onto the surface of catalysts, thereby leaving those charges with opposite polarity to the adsorbed charges in the electrolyte to participate in reactions (Fig. 2d). For tensile stress, piezoelectric particles will undergo a reverse cycle in the adsorption and desorption processes of surface screening charges to participate in reactions.[43] Conclusively, in the theory of the screening charge effect, redox reactions can occur on piezocatalysts through a cycle of polarization-mediated accumulation and release of surface screening charges. Likewise, this effect needs periodic external stress for the continual facilitation of chemical reactions. Furthermore, in the theory of the screening charge effect, the piezoelectrically driven potential is the main driving force for the external charge cycle of release and adsorption. This means that the magnitude of the piezoelectric potential not only determines the feasibility of the piezocatalyst in driving certain specific reactions but is also related to the material's screening charge density, positively correlating with the catalytic efficiency.[44] Additionally, in this mechanism, all
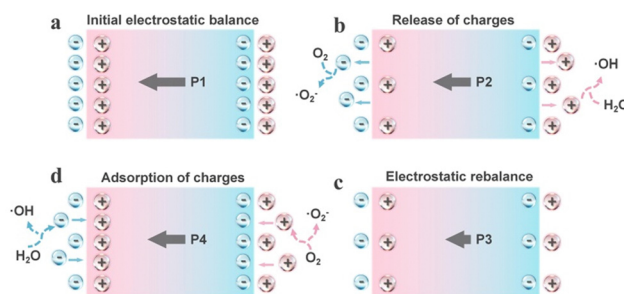

Fig. 2 The schematic description of the screening charge effect of the piezocatalytic mechanism. (a) Initial electrostatic balance. (b) Release of charges. (c) Electrostatic rebalance. (d) Adsorption of charges.
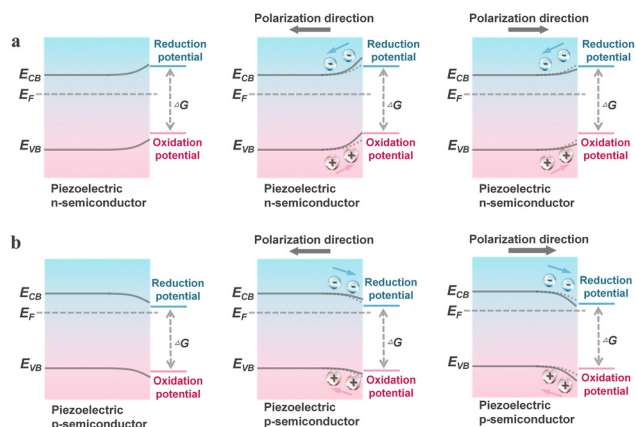
Fig. 3 Interface band bending of (a) n- and (b) p-type piezoelectric semiconductors.

substances present in the reaction environment (such as the chosen solution) will influence the catalytic process (Fig. 3).

2.3 The mechanism of piezo-photocatalysis

As previously mentioned, piezo-photocatalysis based on piezo-phototronics is a process that involves a tri-directional coupling of piezoelectric polarization, photon excitation, and charge separation and transport. The mechanism of piezo-photocatalysis is also very similar to the piezocatalytic mechanism derived from the energy band theory, where externally applied stress-induced piezoelectric polarization can promote the separation and transport of charge carriers and can modulate the energy band structure.[13] However, the modulation of the energy band structure in piezo-photocatalysis is related to the type of piezoelectric semiconductor. When an n-type piezoelectric semiconductor is influenced by negative piezoelectric polarization charges at the interface with the reactant, the energy bands bend upwards, thereby facilitating oxidation reactions. If the interface is influenced by positive piezoelectric polarization charges, the energy bands bend downwards, thereby facilitating reduction reactions. For p-type piezoelectric semiconductors, the situation is exactly the opposite of n-type piezoelectric semiconductors. This means that stress-driven piezoelectric polarization can still alter the inherent redox capabilities of the valence and conduction bands of the piezo-photocatalyst. Similar to the piezocatalytic process, the presence of cycles of externally applied tensile and compressive stress is necessary for the continuous enhancement of the photocatalytic process by piezoelectric polarization.

3. Piezocatalysis for value-added chemical synthesis

In the backdrop of accelerating global industrialization, the synthesis of chemicals is essential to industrial production.[45] Nevertheless, conventional methods of chemical synthesis present an array of environmental issues.[46] Notably, the effluent from acid–base neutralization contaminates aquatic environments, while the gaseous by-products of redox reactions pollute the atmosphere. Such environmental ramifications present significant impediments to the sustainable advancement of human society. Given these challenges, the technique of piezocatalysis for chemical synthesis has garnered increasing attention. This method capitalizes on mechanical energy to induce a polarization field, thereby enabling the separation of electrons and holes.[47] Subsequently, these migrate to the catalyst's surface, facilitating redox reactions.[48] As a result, piezocatalysis exhibits considerable potential in the realm of chemical production, offering a promising pathway towards more environmentally-conscious industrial processes.[49]

3.1 Piezocatalytic synthesis of hydrogen peroxide

Hydrogen peroxide is a significant industrial commodity, utilized for sterilization, medical disinfection, and as an oxidizing agent.[50] Conventionally, the anthraquinone process is employed for the synthesis of H_2O_2, which capitalizes on the property of quinone substances to undergo hydrogenation reduction and subsequent reversion to quinones.[51] In this method, alkylated anthraquinone derivatives serve as carriers and are hydrogenated under the influence of a catalyst, followed by oxidation to yield hydrogen peroxide. However, the reaction conditions for this process are typically stringent, and the synthesis may involve the use of harmful chemical reagents, potentially leading to environmental pollution.[52] In contrast, the piezocatalytic synthesis of hydrogen peroxide represents an emerging method. Compared to the conventional anthraquinone process for H_2O_2 production, the piezocatalytic approach eliminates the need for hazardous chemicals and operates under mild reaction conditions without high temperature or pressure, offering enhanced safety.[53] Consequently, the synthesis of H_2O_2 using piezocatalytic technology has become a burgeoning topic of contemporary research.[54]

Graphitic carbon nitride (g-C_3N_4), a non-metallic polymeric material primarily composed of carbon and nitrogen elements, possesses a cyclic structure enriched with pyridinic nitrogen sites. These sites have been demonstrated to be active sites for oxygen adsorption and activation.[55] Non-metallic g-C_3N_4 is also considered an ideal material for the production of H_2O_2 via the piezocatalytic process.[56] Wang *et al.* experimentally substantiated the piezocatalytic function of graphitic carbon nitride.[57] The layered structure of graphitic carbon nitride and the asymmetric triangular voids on its plane are identified as the sources of piezoelectric effect. The ultrasonically derived piezoelectric polarization of graphitic carbon nitride occurs along its plane, a conclusion supported by Au deposition experiments. The generated piezoelectric polarization field serves as the driving force for the directional migration of electrons. Owing to the piezocatalytic properties of graphitic carbon nitride, the material achieves a hydrogen peroxide production rate of 34 μmol^{-1} h^{-1} under ultrasonic conditions. It is noteworthy that, potentially due to the disruption of the integrity of the triangular holes on the g-C_3N_4 plane, the piezoelectric effect and the piezocatalytic H_2O_2 production rate of g-C_3N_4 with C and N vacancies are inferior to those of the pristine g-C_3N_4.
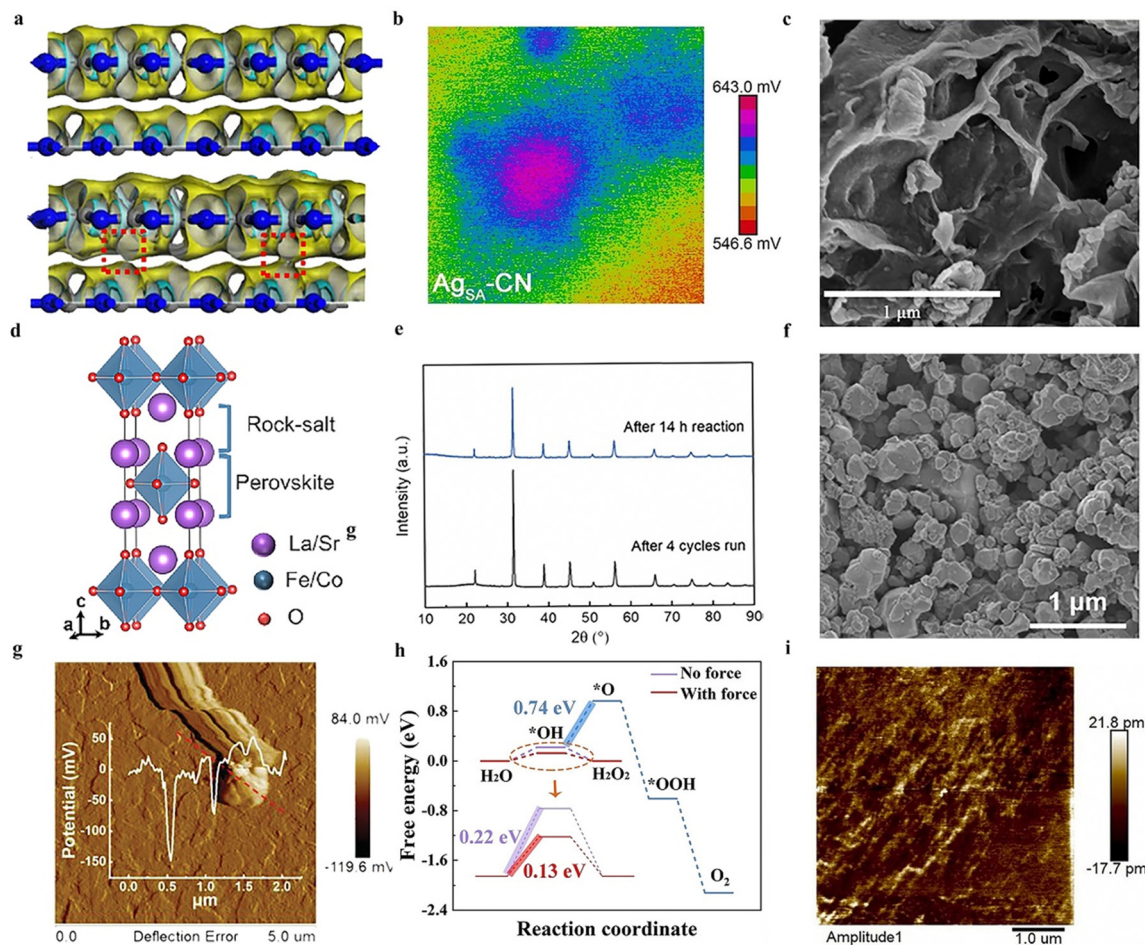
Fig. 4 (a) The different colored regions (yellow and blue) refer to the net electron accumulation and depletion while the isosurface value is 0.017 e Å^{-3}. Apparent charge-transfer channels as marked by red rectangles can be observed for g-C$_3$N$_4$/g-C$_3$N$_{4-x}$S$_x$.[58] Copyright 2022 Zhengzhou University. (b) The potential maps of single Ag atoms are anchored on graphitic carbon nitride.[61] Copyright 2022 Wiley-VCH GmbH. (c) SEM image of two-dimensional layered C$_3$N$_5$ containing O sites and N vacancies.[64] Copyright 2022 Elsevier B.V. (d) Ruddlesden–Popper perovskite phase.[65] Copyright 2023 Elsevier B.V. (e) XRD patterns of recycled four processes BCZT-0.5.[66] Copyright 2022 Elsevier Ltd. (f) The FESEM image of Ag-loaded Bi$_{0.5}$Na$_{0.5}$TiO$_3$-AgNbO$_3$.[67] Copyright 2023 Elsevier B.V. (g) Surface piezoelectric potentials of C-layer coated ZnO.[68] Copyright 2023 Wiley-VCH GmbH. (h) Free energy diagram for two-electron or four-electron water oxidative H$_2$O$_2$ production on BiOIO$_3$.[69] Copyright 2023 Wiley-VCH GmbH. (i) PFM of HAP amplitude image.[70] Copyright 2022 Elsevier B.V.

Building upon graphitic carbon nitride, Xu *et al.* developed a crystalline g-C$_3$N$_4$/g-C$_3$N$_{4-x}$S$_x$ homojunction heterostructure using the molten salt method.[58] The synthesis involved the thermal polymerization of thiourea in air, thereby enabling the incorporation of sulfur species to enhance the degree of polymerization. Apparent charge transfer channels are formed in the S-doped g-C$_3$N$_4$ (Fig. 4a). This structure exposes more active sites, augmenting the catalytic activity for reactants. Consequently, the material exhibits exceptional reactivity in the generation of H$_2$O$_2$. Furthermore, experimental evidence suggests that this homojunction heterostructure, upon treatment with NaBH$_4$, introduces additional cyano groups and eliminates NHx groups. This results in an enhanced asymmetric structure, thereby further augmenting the piezocatalytic activity, leading to a higher yield of H$_2$O$_2$.

The piezocatalytic performance of g-C$_3$N$_4$ materials can generally be further modified through various methods.[59] The loading of single atoms has emerged as an effective approach to enhance catalytic performance, a technique also applicable to improving the piezocatalytic hydrogen peroxide production capabilities of g-C$_3$N$_4$ materials.[60] For instance, Hu *et al.* reported a piezocatalytic system for H$_2$O$_2$, wherein single Ag atoms are anchored on graphitic carbon nitride, serving as multifunctional sites for efficient two-electron water splitting to produce H$_2$O$_2$.[61] Experimental observations indicate that the coordination of single Ag atoms with C and N atoms significantly enhances the in-plane piezoelectric polarization of CN due to charge redistribution (Fig. 4b). The improved charge transfer and reduced reaction barriers can elevate the piezocatalytic performance of the material, thereby resulting in higher H$_2$ and H$_2$O$_2$ production rates.

C$_3$N$_5$ is part of a class of carbon-nitrogen compounds, generally derivatives of g-C$_3$N$_4$ (graphitic carbon nitride).[62] C$_3$N$_5$, a porous nitrogen-rich carbon-based solid material,

exhibits high specific surface area, and excellent thermal and chemical stability, hence demonstrating potential catalytic efficacy.[63] Fu et al. synthesized two-dimensional layered C_3N_5 containing O sites and N vacancies through a strategy of thermal polymerization and thermal etching (Fig. 4c), and reported on the piezoelectric properties of this material.[64] The thermal etching process aids in forming thin layers and porous structures, exposing more triangular holes and thereby enhancing the piezoelectric properties of the material. Furthermore, defect engineering effectively amplifies the asymmetry of the catalyst's molecular structure, also improving the polarization and piezoelectric performance of the catalyst. Consequently, experimental results indicate that even in the absence of a sacrificial agent, this material can efficiently generate H_2O_2 at a rate of 0.615 mM g^{-1} h^{-1} within the piezoelectric system.

Perovskite materials are a class of critically important piezoelectric materials, with inorganic perovskites being one of the main components of piezoelectric materials.[71] Their typical characteristic is the molecular formula ABX_3 (where A and B are cations, and X is an anion).[72] Taking the inorganic perovskite $BaTiO_3$ as an example, when an external force is applied, the Ti atoms in the center of the TiO_6 octahedra are displaced, altering the original charge distribution and generating polarization.[73] Hence, a piezoelectric potential distributed along the direction of the stress is produced, endowing the material with piezoelectric effects.[74] Based on their excellent piezoelectric effects, similar ABX_3-type inorganic perovskite metal oxides are increasingly being used in the piezocatalytic production of H_2O_2. He et al. reported on a doped C $KNbO_3$ nanocrystal serving as a piezocatalyst for the production of H_2O_2.[75] Piezoresponse force microscopy (PFM) results indicate that doping with C significantly enhances the piezoelectric response of $KNbO_3$, facilitating the separation of free charge carriers and achieving higher piezocatalytic efficiency. Additionally, it is noteworthy that the synthesized 0.5 : 1 C-$KNbO_3$ is capable of efficiently generating both H_2 and H_2O_2 simultaneously. Traditional piezocatalysts often face limitations in their efficiency due to low piezoelectricity.[76] Fang et al. developed a piezocatalyst for H_2O_2 production using Ruddlesden–Popper (R–P) type perovskites composed of La, Sr, Co, and Fe, synthesized via the conventional sol–gel method (Fig. 4d).[65] The relatively lower oxygen vacancy in the Ruddlesden–Popper phase ($LaSrFeO_4$ and $LaSrCoO_4$) eliminates the attenuation effect of polarization domain reversal, thereby exhibiting higher piezoelectricity compared to the single perovskite phase, enhancing the efficiency of H_2O_2 production. Additionally, experiments demonstrated that iron-containing catalysts exhibit superior piezocatalytic performance compared to those containing cobalt.

Some perovskites, due to their suboptimal piezoelectric properties, result in less than ideal yields of H_2O_2. By modifying themselves and constructing composite materials, the inherent shortcomings of piezoelectric properties can be effectively compensated for.[66] Wang et al. reported a method to enhance piezoelectricity by introducing more favorable crystal phases.[66]

A ternary BaCaZrTi perovskite oxide piezocatalyst is prepared by them. Owing to the coexistence of its ternary phases (orthorhombic, tetragonal, and rhombohedral), the barrier for polarization rotation is reduced, significantly enhancing its piezoelectric performance. Under ultrasonic irradiation, the rate of H_2O_2 production reached 692 μmol g^{-1} h^{-1}, demonstrating exceptional selectivity for H_2O_2 generation and sustained stability (Fig. 4e). Piezocatalysis holds significant potential as an alternative to the traditional anthraquinone process for hydrogen peroxide production, but key challenges to be addressed include enhancing the efficiency of mechanical energy conversion and increasing the number of active sites on the surface.[67] Zhang et al. employed a two-step high-temperature solid-state reaction method to synthesize an Ag-loaded $Bi_{0.5}Na_{0.5}TiO_3$–$AgNbO_3$ solid solution for dual-channel H_2O_2 production (Fig. 4f).[67] Experimental evidence suggests that surface Ag, acting as a co-catalyst, enhances the piezocatalytic redox reactions, while the reduction of surface hydroxyl groups results in more active sites for water oxidation on the material's surface. Moreover, phase structural changes induced by Ag and Nb enable the material to utilize minimal mechanical forces. These factors contribute to the material's excellent piezoelectric performance, making it an outstanding piezocatalyst for hydrogen peroxide production.

Besides the typical perovskite metal oxides, other low-cost piezoelectric metal oxide materials with non-centrosymmetric structures have been developed as catalysts for piezocatalytic production of H_2O_2.[77,78] Wen et al. constructed a C-layer coated ZnO with a modulated electronic structure, employing it in piezocatalytic H_2O_2 generation.[68] The interface interaction between the C layer and ZnO modulates the charge distribution at the active centers, and the excellent conductivity of C enhances the surface piezoelectric potential and piezoelectric effect of the material compared to ZnO (Fig. 4g). Experiments demonstrated that this material achieved an ultra-high H_2O_2 production rate of 294 μM h^{-1} through a single-electron water oxidation process. Introducing appropriate oxygen vacancies in anti-spinel materials can enhance active sites, facilitate charge transfer, and accelerate redox reactions, thereby improving piezocatalytic activity.[79] In light of this property, Yao et al. successfully synthesized $NiFe_2O_4$ nanofibers with tunable oxygen defects using defect engineering techniques.[80] Experimental evidence indicates that the material achieves a green production rate of H_2O_2 of 570 μmol L^{-1}, an increase of 39%. This enhancement is attributed to the presence of oxygen defects, which raise the rate of charge transfer and the utilization of free radicals, providing more reactive sites for the catalytic process. Therefore, it elevates the efficiency of piezocatalytic H_2O_2 production.

Bismuth-based compounds are a category of piezoelectric materials receiving attention for their low toxicity and abundant availability.[81] Xu et al. successfully constructed a novel Fe^{III}/$BiOIO_3$ piezocatalytic self-Fenton system and applied it for two-electron water oxidative H_2O_2 production.[69] The appropriate piezoelectric potential difference of $BiOIO_3$ effectively overcomes the high thermodynamic barrier of two-electron water

oxidative H_2O_2 production (Fig. 4h). Additionally, the added Fe^{III} further facilitates H_2O_2 generation. This system demonstrates potential in piezocatalytic H_2O_2 production. Notably, compared to the typical $BiOIO_3/Fe^{II}$ piezocatalytic Fenton system, it exhibits a faster Fe^{III}/Fe^{II} cycle and a higher $^\bullet OH$ production rate. Wei et al. reported on an iron-loaded bismuth vanadate material, whose piezoelectricity is confirmed via piezoresponse force microscopy.[82] In experiments, this material is used as a catalyst for piezocatalytic H_2O_2 production. The loading of Fe increased the carrier density, thus enhancing the piezocatalytic activity for the generation and activation of H_2O_2. Additionally, Fe on the material's surface exhibited mixed valence states ($Fe(II)$ and $Fe(III)$), promoting the production of $^\bullet OH$. The generation of $^\bullet OH$ further degraded chlorophenol, a fact substantiated by ultra-high-performance liquid chromatography–mass spectrometry analysis. Defect engineering is one of the most common strategies in the field of catalysis, effectively modulating the electronic structure and surface state of catalysts to enhance their catalytic performance. Wang et al. employed surfactant-assisted hydrothermal synthesis coupled with post-reduction treatment to fabricate ultra-thin $Bi_4Ti_3O_{12}$ nanosheets with atomic-level thickness and surface oxygen vacancies.[83] PFM testing indicated that the production of atomic-level thickness nanosheets could enhance the piezocatalytic activity of $Bi_4Ti_3O_{12}$, and the introduction of surface oxygen vacancies further improved its piezocatalytic activity. Experiments demonstrated that this material exhibited exceptional piezocatalytic performance in generating H_2O_2, achieving a yield of 161.12 μmol in 2 hours. The combination of materials with different lattice structures, chemical compositions, or properties may facilitate energy matching between the redox potentials and band structures of the materials, achieving enhanced piezocatalytic performance.[84] Ma et al. utilized solid-state sintering technology to fabricate a novel heterostructure piezocatalyst of $RbBiNb_2O_7$/polytetrafluoroethylene (PTFE) for the catalytic production of H_2O_2.[85] The piezoelectric polarization of PTFE induced a band bending in $RbBiNb_2O_7$, leading to an energy match between the required redox potentials and the band structure of $RbBiNb_2O_7$, which is favorable for H_2 and $^\bullet OH$-mediated H_2O_2 generation. Experiments showed that the modified $RbBiNb_2O_7$ exhibited a several-fold increase in the piezocatalytic H_2O_2 production rate compared to the pristine $RbBiNb_2O_7$.

Piezocatalysts must not only possess excellent piezoelectric properties but also demonstrate good catalytic performance for the anticipated catalytic reactions.[86] Therefore, the exploration of piezocatalysts that simultaneously possess piezoelectric properties and outstanding catalytic characteristics is crucial for the advancement of the piezocatalysis.[87] Jia et al. reported on the task of piezocatalytic hydrogen peroxide generation using piezocatalysts made of three different compositions of MAX phases: Ti_3AlC_2, Ti_3AlCN, and Ti_3SiC_2.[88] The MAX phase catalysts also demonstrated high-efficiency piezocatalytic activity. Studies show that the efficient H_2O_2 generation by MAX phases is achieved through a two-electron transfer pathway, facilitating both water oxidation and oxygen reduction

processes. Notably, due to the significant piezoelectric performance of Ti_3SiC_2, characterized by reduced electron transfer resistance and high free charge density, Ti_3SiC_2 out of the three MAX materials studied exhibited the highest piezocatalytic activity for H_2O_2 production. Metal–organic frameworks (MOFs), composed of organic ligands and metal ions through self-assembly, are recognized as promising alternatives to traditional piezoelectric/ferroelectric materials due to their exceptionally large specific surface area, high porosity, high transition metal content, and chemically tunable structures.[89] However, research often overlooks the influence of elemental properties and electronic states on the metal–ligand centers in these frameworks. Li and colleagues synthesized different metal center sites in MOFs, including MIL-101(Cr) and MIL-101(Fe), for piezocatalytic production of H_2O_2.[90] Experimental results demonstrated that the H_2O_2 production rate of MIL-101(Cr) is 2.76 mmol g^{-1} h^{-1}, while that of MIL-101(Fe) is 1.31 mmol g^{-1} h^{-1}, surpassing most piezocatalytic processes. Hydroxyapatite, a widely used eco-friendly material known for its excellent biocompatibility and rich physicochemical properties, has been extensively studied in recent years.[91] However, its piezoelectric characteristics have not been thoroughly investigated. Yin and colleagues reported a study on the piezoelectric properties of hydroxyapatite, demonstrating its capability in piezocatalytic H_2O_2 production.[70] Experiments utilizing PFM revealed different polarizations within the material, confirming the generation of an internal piezoelectric field (Fig. 4i). Additionally, under ultrasonic treatment, the accumulated concentration of H_2O_2 reached 152.24 μmol L^{-1} within 30 minutes, with the produced H_2O_2 exhibiting stable properties. To conclude, a growing number of novel piezocatalysts, which are different from traditional piezoelectric materials, have been developed in recent years for the production of hydrogen peroxide through piezocatalysis technology.

3.2 Piezocatalysis for carbon dioxide reduction

In contemporary society, with the extensive consumption of fossil fuels leading to increased carbon dioxide emissions, addressing how to mitigate CO_2 to avert the greenhouse effect has emerged as a pressing concern.[92] The general consensus is that harnessing renewable energy to convert carbon dioxide into value-added chemical feedstock presents a viable solution.[93] Piezocatalysis is an innovative green technology that does not require supplementary electrical or light energy and can utilize low-frequency mechanical energy. Consequently, piezocatalysis may emerge as an environmentally friendly technique for the reduction of CO_2.[94] As such, current research is delving deeply into the role of the piezoelectric field in the piezocatalytic reduction of CO_2.[95]

Lead-free piezoelectric materials, as eco-friendly alternatives, exhibit environmentally friendly characteristics compared to traditional lead-based piezoelectric materials, such as lead zirconate titanate (PZT).[96] Moreover, many lead-free materials have already demonstrated performance on par with or even superior to traditional materials.[97] Barium titanate ($BaTiO_3$) is a widely used ceramic material in piezoelectrics.[98] Upon the

application of an electric field, the displacement of titanium ions from the central position causes the crystal unit to become polarized, thereby generating a piezoelectric effect.[99] Ma *et al.* proposed a piezocatalytic CO_2 reduction method driven by vibration using $BaTiO_3$.[23] This catalyst provides suitable piezoelectric potential, overcoming the redox potential of CO_2 and reducing the free energy during vibration. It achieves nearly 100% selectivity in reducing CO_2 to CO, with the highest CO yield reaching up to 63.3 µmol g^{-1}. Combining a Co–N–C composite material with $BaTiO_3$ forms a novel piezocatalyst (Fig. 5a). This material merges the piezoelectric properties of $BaTiO_3$ with the catalytic activity of Co–N–C to accelerate chemical reactions.[100] Ren and colleagues utilized this material as a piezocatalyst for CO_2 reduction reactions.[95] Electrons generated by the driven piezoelectric effect transfer from $BaTiO_3$ to Co–N–C, and surface piezoelectric potential has been formed (Fig. 5b). The band structure of $BaTiO_3$ meets the reaction potential, facilitating electron transfer at active sites for CO_2 reduction. Additionally, under ultrasonic frequency conditions of 50 kHz, the highest CO yield reached 261.8 µmol g^{-1} h^{-1}, with a CO selectivity of up to 93.8%.

Similarly, with the development of piezoelectric materials, other lead-free piezoelectric materials have also been developed.[101] For instance, Phuong *et al.* utilized lead-free lithium-doped potassium sodium niobate ferroelectric ceramic particles for the piezocatalytic reduction of CO_2 (Fig. 5c).[102] Ultrasonic waves apply mechanical pressure to the ferroelectric particles, generating surface charges through the piezoelectric effect, which act as the driving force for the piezoelectric reaction (Fig. 5d). Experiments demonstrate that an exceptionally high piezocatalytic CO_2 reduction rate of 438 µmol g^{-1} h^{-1} can be achieved at suitable gaseous CO_2 concentration and optimal catalyst loading. Conversely, further increasing the dosage reduces the selectivity of CO_2 reduction due to the
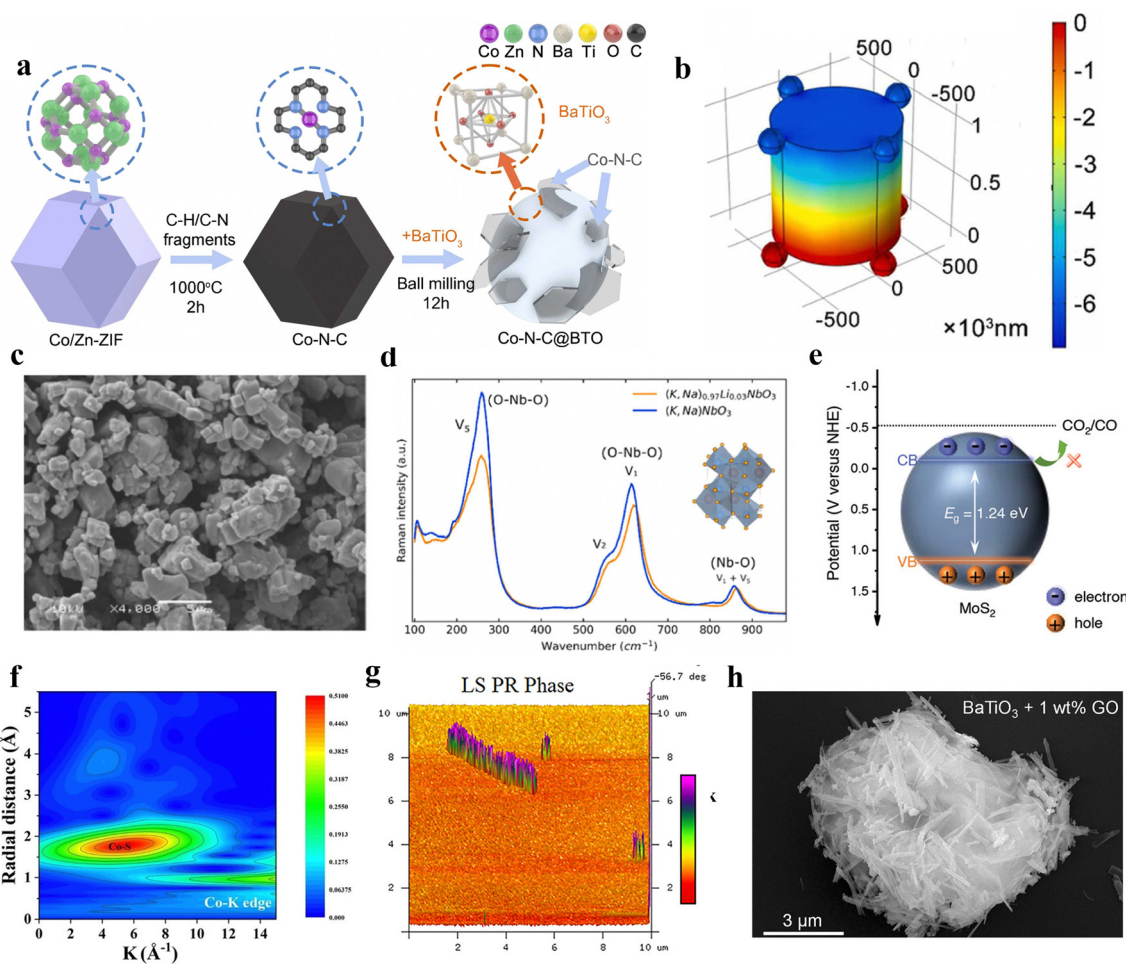

Fig. 5 (a) Schematic of the Co−N−C@BTO synthesis process.[23] Copyright 2022 Elsevier B.V. (b) The piezoelectric potential upon the surface of Co−N−C@BTO. BTO with irregular morphology is equivalent to a cylinder, and the Co−N−C particles are equivalent to a nanosphere.[95] Copyright 2022 Elsevier B.V. (c) SEM image of the lead-free lithium-doped potassium sodium niobate ferroelectric ceramic powder.[102] Copyright 2022 Elsevier Ltd. (d) Raman spectrum of the lead-free lithium-doped potassium sodium niobate ferroelectric ceramic powders.[102] Copyright 2022 Elsevier Ltd. (e) The band structure of MoS_2 nanoflakes *versus* normal hydrogen electrode NHE at pH 7.[103] Copyright 2023 Wiley-VCH GmbH. (f) The Co K-edge k^2-weighted WT-EXAFS.[104] Copyright 2023 Wiley-VCH GmbH. (g) Phase images of the SnS nanobelt.[105] Copyright 2023 Wiley-VCH GmbH. (h) SEM images of $BaTiO_3$ + 1 wt% GO.[106] Copyright 2023 Elsevier Ltd.

decreased number of active CO_2 species under high alkalinity conditions.

Transition metal dichalcogenide crystals, such as MoS_2, WS_2, WSe_2, and $MoSe_2$, are typical two-dimensional piezoelectric materials.[107] These crystals possess a centrally symmetric hexagonal lattice arranged in a triangular pattern, similar to monolayer crystals, are asymmetrically arranged, lack inversion centers, and exhibit asymmetric charge density distribution, thereby exhibiting piezoelectric effects.[108] Ma et al. reported on the synthesis of molybdenum disulfide nanosheets via a hydrothermal method, which were then utilized in the piezocatalytic reduction process of carbon dioxide.[103] The experiment demonstrated that this material independently completes the entire carbon cycle chain from CO_2 capture to conversion, achieving an ultrahigh purity piezocatalytic CO production rate of 543.1 μmol g^{-1} h^{-1}. However, it is noteworthy that, during the reaction, the conduction band does not shift to the potential required for the CO_2 to CO conversion (Fig. 5e). This also substantiates that the piezocatalytic mechanism of the reaction is distinct and independent of the band position. Furthermore, MoS_2 nanoflakes exhibit an unexpectedly strong 'breathing' effect under vibration, capable of independently completing the entire carbon cycle chain from CO_2 capture to conversion. It must be noted that this work is groundbreaking in the exploration of the mechanism of piezocatalysis, providing a very important guide to the band theory and the mechanism of the screening charge effect in piezocatalysis. That is, for piezoelectric catalysts with a narrow band gap, their piezocatalysis mechanism might be unrelated to the band theory. Essentially, the carbon dioxide reduction reaction (CRR) is vital for pointing out this mechanism, as the reactions at the gas–solid–liquid triple-phase interface greatly minimize the interference of sonochemistry in exploring the mechanism. This also reflects the important role of piezocatalysis in the synthesis of chemicals within the field of piezocatalysis.

The coupled system of piezocatalysis and advanced oxidation processes (AOPs) is an emerging technology that combines the characteristics of piezocatalysis with the efficiency of advanced oxidation processes.[109] Ran and colleagues successfully developed a coupled system of piezocatalysis and advanced oxidation processes, utilizing the excellent piezoelectricity of molybdenum disulfide (MoS_2) and the superior peroxymonosulfate activation efficiency of cobalt-based catalysts to achieve low carbon emission wastewater treatment.[104] Due to the synergistic effects of improved charge separation/transfer and the more favorable thermodynamic reaction from carbonate to Co_3S_4/MoS_2, the CO production rate is notably superior with MoS_2. The EXAFS wavelet transforms highlighted the presence of Co–S bonds (Fig. 5f). Additionally, this work also elucidated the mechanism of phenol conversion to CO, where phenol is first oxidized to carbonate by peroxymonosulfate activation and then reduced to CO by piezoelectric electrons.

Converting carbon dioxide into high-value C2 chemicals like acetates represents a significant and viable pathway towards sustainable development.[110] The controlled hydrogenation with simultaneous C–C bond formation significantly increases

the difficulty of converting CO_2 into C2+ chemicals compared to C1 chemicals.[111] Among these, transition metal dichalcogenides, as piezocatalysts, offer a new approach to addressing this challenge. Tian et al. have synthesized a vibration-driven tin disulfide nanoribbon, and phase images indicate that this material exhibits a piezoelectric response (Fig. 5g).[105] The piezocatalysis efficiently converts carbon dioxide into acetate with 100% selectivity, and demonstrates a considerably high yield. This indicated that the band gap of SnS nanoribbons decreases, and the reduction in the distance between Sn atoms leads to charge accumulation at the active sites, thereby facilitating CO_2 activation and C–C coupling. This in turn lowers the reaction barriers for producing products like acetates.

Given the extensive research on piezoelectric materials, there is an urgent need for the rapid, large-scale fabrication of efficient, low-cost piezocatalysts. Combining them with abundant carbon-based materials on Earth may be a pathway to resolve this challenge.[112] Ma et al. physically mixed the typical piezoelectric material $BaTiO_3$ with graphene oxide, employing it as a piezocatalyst for CO_2 reduction.[106] After mixing $BaTiO_3$ with GO, it can be found that the nanofibers and nanosheets are tightly connected (Fig. 5h). At an appropriate concentration of graphene oxide, $BaTiO_3$ exhibited a CO production rate of 134.4 μmol g^{-1} h^{-1} with a selectivity near 100%. This combination significantly enhanced the piezoelectric carrier dynamics of $BaTiO_3$.

3.3 Piezocatalytic nitrogen to value-added chemicals

The Haber–Bosch process is the most common method for synthesizing ammonia, but due to its requirement for high temperatures and pressures, it is relatively costly.[116] In recent years, the focus of ammonia synthesis research has primarily shifted to directly converting N_2 and water into ammonia under ambient conditions using light or electricity. The main challenge of this technology is to provide the reduction potential necessary for breaking the N_2 bond.[117] The piezoelectric process can supply the high electrostatic potential required for this process, making the use of piezoelectric reactions for synthesizing ammonia a growing research trend. Peng et al. constructed a material comprising silver nanoparticles loaded onto zinc oxide microrods (Fig. 6a and b).[113] The oxygen vacancies on the surface of ZnO serve as active sites for the adsorption and activation of N_2. Additionally, due to the formation of local strain at the Ag–ZnO interface, the chemical interaction between N_2 and Ag is strengthened, facilitating carrier separation and enhancing the catalytic activity of the sample. Ning et al. synthesized a high-performance CuS/ZnO Z-scheme heterostructure piezoelectric catalyst using solid-state chemical methods (Fig. 6c).[114] Among them, ZnO has a hexagonal wurtzite structure (Fig. 6d). This composite sample effectively promotes the efficient migration and separation of charge carriers, thereby exhibiting excellent piezocatalytic performance. The CuS/ZnO Z-scheme heterostructure demonstrated the capability to reduce N_2 to NH_3, showcasing high nitrogen fixation yields and stability. The average NH_3 production rate is approximately 77.5 μmol L^{-1} g_{cat}^{-1} h^{-1}, which is significantly
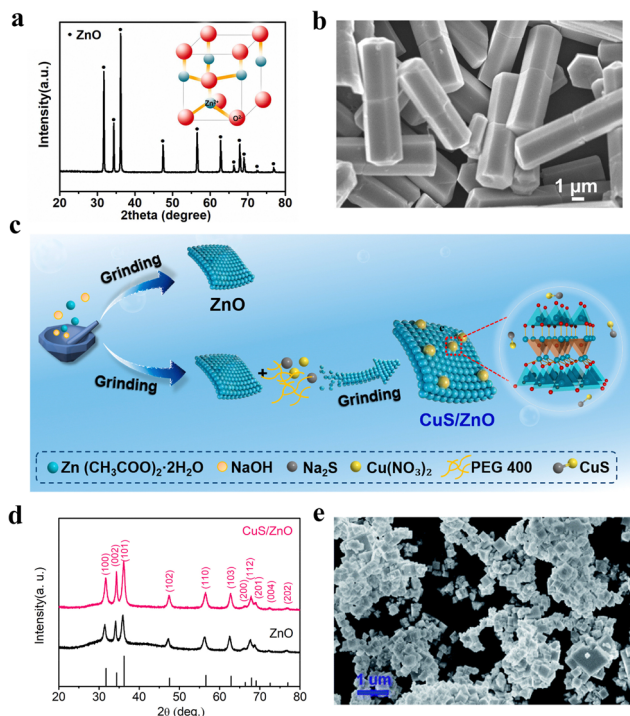
Fig. 6 (a) XRD pattern of ZnO microrods. (b) FESEM of ZnO microrods.[113] Copyright 2022 Elsevier Ltd. (c) Schematic diagram of the synthetic processes of ZnO and CuS/ZnO. (d) XRD patterns of as-synthesized ZnO and CuS/ZnO.[114] Copyright 2023 Elsevier Ltd and Techna Group S.r.l. (e) SEM images of $KTa_{0.75}Nb_{0.25}O_3$.[115] Copyright The Royal Society of Chemistry 2021.

higher than that of ZnO alone. This research indicates that the CuS/ZnO Z-scheme heterostructure holds considerable potential in the piezoelectric-catalyzed synthesis of ammonia.

Chen and colleagues developed a novel material for piezoelectric ammonia synthesis, fabricating a $Bi_2S_3/KTa_{0.75}Nb_{0.25}O_3$ heterojunction nanocomposite using a two-step hydrothermal method.[115] Among them, $KTa_{0.75}Nb_{0.25}O_3$ possesses a morphology of nanocubes (Fig. 6e). The addition of Bi_2S_3 captures the piezoelectric electrons from $KTa_{0.75}Nb_{0.25}O_3$, enhancing the spatial separation efficiency of electron–hole pairs and prolonging the lifetime of negative charges generated by the piezoelectric effect. Since $KTa_{0.75}Nb_{0.25}O_3$ is inherently an effective piezocatalytic material, the $Bi_2S_3/KTa_{0.75}Nb_{0.25}O_3$ heterojunction nanocomposite demonstrates high efficiency in piezocatalytic ammonia synthesis.

3.4 Piezocatalysis for the synthesis of organic chemicals

Mechanical force and chemical reactions are coupled together as the main approach for the piezocatalysis synthesis of organic chemicals.[118] Piezoelectric materials can serve as catalysts for redox reactions in mechanochemical organic synthesis.[119] High-energy ball milling, ultrasonication, or the cavitation effect of liquids can be used to cleave the covalent bonds of organic molecules or polymers. At the same time, the piezocatalytic process can combine mechanochemical redox catalysis with transition metal catalysis to control the conformation of complex molecules.[120] The typical approach involves using piezoelectric barium titanate material as a catalyst and triggering single-electron transfer redox reactions through the mechanical stress of ball milling, generating radicals for further organic reactions. Under the influence of mechanical energy, various arylation reactions are successfully initiated (Fig. 7a).[121] In the piezocatalytic process, the piezocatalyst is a mature material with good recyclability and relatively low cost.[122] Moreover, the scope of this piezocatalysis can be extended to polymerization reactions, degradation reactions, recycling, and other free radical-related chemical reactions. These extensive applications will drive efforts to develop more efficient piezoelectric materials for the synthesis of organic chemicals driven by mechanical energy.[123]

The advantages of mechanochemical synthesis using ball milling include avoiding potentially harmful organic solvents and external heating, shorter reaction times, and simpler processing.[124] Stirring piezoelectric materials *via* ball milling can generate transiently highly polarized particles, which as strong reductants transfer electrons to small organic molecules, subsequently quenching the donor through oxidation, thus inducing the formation of chemical bonds in a manner similar to photo-redox processes. Ito's research group used inexpensive and readily available $BaTiO_3$ nanoparticle piezoelectric materials as catalysts, achieving breakthrough progress in the field of mechanochemical synthesis (piezocatalysis synthesis).[125] Mechanical stirring of $BaTiO_3$ in a ball mill can generate an appropriate electrochemical potential, thereby activating small redox-active organic molecules in organic synthesis. By a mechanism of single-electron transfer (SET) similar to photo-redox reactions, the aryl diazonium salt (1) is reduced (Fig. 7b), generating the corresponding aryl radical I. The addition of I to the heteroarene 2 produces the radical addition intermediate II, which is subsequently oxidized by the activated holes in $BaTiO_3$ to form the carbocation intermediate III. Finally, the deprotonation of III yields the arylated product 3. In the borylation reaction, the generated radical I reacts with bis(pinacolate)diboron (4), cleaving the B–B bond to form the boron-substituted product 5 and the radical anion intermediate IV. Subsequently, IV is oxidized by the activated $BaTiO_3$ to form F–B(pin) (V).

Similarly, the first application of piezoelectricity in the generation of trifluoromethyl (CF_3) radicals is also reported by Ito's research group.[126] This application, compared to traditional solution-based methods, allows for a cleaner mechanical piezoelectric redox C–H trifluoromethylation that can be conducted in air, without the need for large amounts of dry and degassed organic solvents, nor specific processing techniques. This work established a mechanochemical method for C–H trifluoromethylation of aromatic compounds, where CF_3 radicals are generated by piezoelectric reduction during the ball milling process. The generated radicals are then added to aromatics to obtain trifluoromethylated intermediates, which are then oxidized by holes in the stirred $BaTiO_3$, followed by deprotonation to yield the product. Inspired by predecessors, Wang *et al.* used piezoelectric materials as redox catalysts
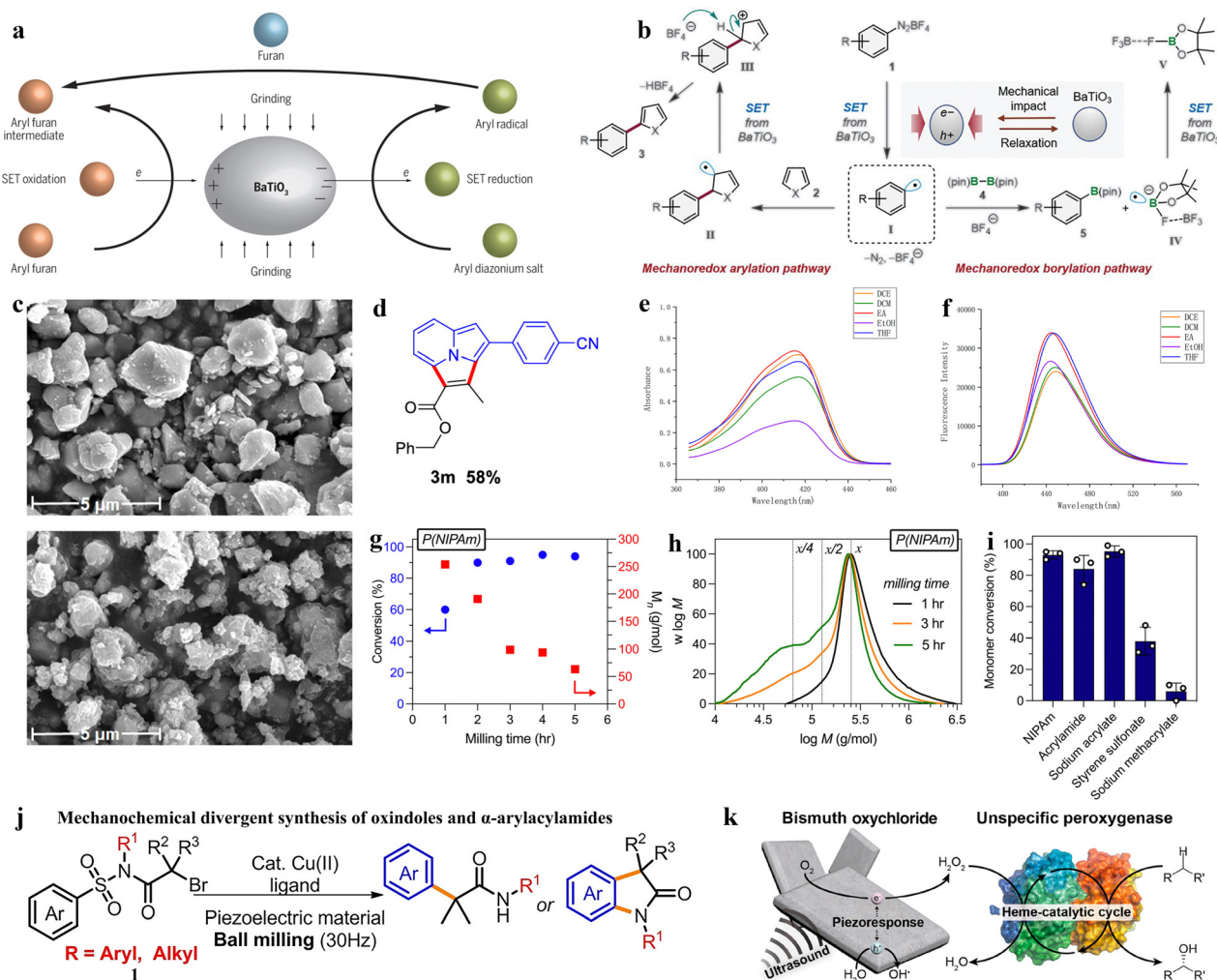
Fig. 7 (a) Grinding piezoelectric barium titanate (BaTiO₃), aryl diazonium salt, and furan with a ball mill allows organic synthesis of aryl furan compounds.[121] Copyright 2019, The American Association for the Advancement of Science. (b) Proposed mechanism for the mechanoredox arylation and borylation using BaTiO₃ and ball milling.[125] Copyright 2019, The American Association for the Advancement of Science. (c) SEM of BaTiO₃ particles before and after fluorination.[127] Copyright 2023 Wiley-VCH GmbH. (d) Compound 3m (benzyl 3-(4-cyanophenyl)-2-methylpyrrolo[2,1,5-cd]indolizine-1-carboxylate). (e) Ultraviolet-visible absorption spectra. (f) Fluorescence (excited at λ_{max}) spectra of 3m.[129] Copyright 2022 American Chemical Society. (g) Monomer conversion values for a range of solid vinyl monomers through ball milling with BaTiO₃. (h) Mechanochemical divergent syntheses of oxindoles and α-arylacylamides. (i) Schematic illustration of piezobiocatalytic oxyfunctionalization reactions by BiOCl–rAaeUPO Hybrida.[130] Copyright 2023 The Authors. Angewandte Chemie International Edition published by Wiley-VCH GmbH. (j) Mechanochemical divergent syntheses of oxindoles and α-arylacylamides.[131] Copyright 2022 Wiley-VCH GmbH. (k) Piezoelectric BiOCl microsheets induce piezocatalytic reduction of O₂ to H₂O₂ under ultrasonic irradiation. The in situ-generated H₂O₂ activates the redox center of an unspecific peroxygenase to catalyze selective oxyfunctionalization of various organic compounds.[132] Copyright 2020 American Chemical Society.

under selective fluorine presence conditions, and similarly synthesized aryl fluorides from aryl diazonium tetrafluoroborates under ball milling conditions. The mechanochemically polarized piezoelectric material transfers fluorine from selective fluoride to the aryl radical formed by the reduction of aryl diazonium salts, thus forming mechanochemical fluorination of aryl diazonium salts catalyzed by the piezoelectric BaTiO₃ particles (Fig. 7c).[127] Prior to this, Cao's research group reported several effective visible-light-induced systems for constructing functionalized indoles.[128] To enhance the variety of green synthesis methods, a mechanochemically induced method has been introduced in this work which involves the

use of BaTiO₃ as a piezoelectric material to prepare classes of indolizinones and epoxides, synthesizing some 1,2-diketone indolizinone derivatives. This method does not require solvents, features simple experimental operations, holds potential for scalability, and achieves high conversion efficiency, making it a significant approach for the green synthesis of indolizine derivatives. Similarly, in the following year, Cao's research group conducted a study using cubic BaTiO₃ as the piezoelectric material and TFA as an additive in a mechanochemical ball milling system to form the desired products.[129] Then, a set of oxidants such as H₂O₂, TBHP, and (NH₂)₂S₂O₈ are added to the reaction. The study showed that the addition of H₂O₂

significantly increased the yield of pyrroles to about 75%. This reaction, under mechanochemical induction conditions, proceeds through a 3 + 2 cyclization process, employing a broad range of vinyl indole reactions for the indolization of various substituted pyrroles. In this synthesis process, the solvents of the compound are compared in air at 25 °C, where data showed that benzyl 3-(4-cyanophenyl)-2-methylpyrrolo 2,1,5-cd indolizine-1-carboxylate (Fig. 7d) has an absorption wavelength range of 415–417 nm and an emission wavelength range of 444–449 nm in solvents such as DCE, DCM, EA, EtOH, and THF. When using ethyl acetate (EA) as the solvent, the compound exhibited the highest absorption intensity and fluorescence emission intensity (Fig. 7e and f). In this process, the use of piezoelectric materials as charge transfer catalysts significantly enhanced the reaction efficiency.[129]

In the field of mechanochemistry, D. Nothling's team has utilized physical force to drive redox reactions, converting mechanical energy into chemical potential. In the solid state, piezoelectric $BaTiO_3$ nanoparticles are activated by ball milling, hammering, or repeated compression, resulting in the production of highly reactive hydroxyl radicals ($^{\bullet}OH$), which easily leads to the growth of free radical chains and the cross-linking of solid styrene amides, acrylates, methacrylates and styrene monomers. Sodium acrylate, sodium styrene sulfonate, acrylamide, and sodium methacrylate, when ground with $BaTiO_3$ as a mechano-chemical transduction element, are all converted into their respective polymers with varying yields (Fig. 7g–i).[130] Similarly, Liu and colleagues studied the synthesis of aryl radicals from aryl diazonium salts using a mechanochemical single electron transfer strategy induced without solvent or catalyst. They obtained a series of 2-arylquinolines and 3-arylquinoline-2(1H)$^{-}$ones with yields ranging from 28% to 85%.[133] Also in that year, Lv and colleagues used readily available α-bromo N-sulfonyl amides as raw materials, with highly polarized $BaTiO_3$ or $PbTiO_3$ under mechanical stirring acting as electron donors to achieve the recycling of Cu^{2+} and Cu^{1+} (Fig. 7j).[131] This work reports on the combined use of ball milling, piezoelectric materials, and copper catalysis, surpassing the established solid-phase chemistry, for the divergent synthesis process of oxidizing indoles and α-arylated amides.

In terms of utilizing mechanochemical effects, Song exploited the properties of piezoelectric barium strontium sulfate (BSS), harnessing the mechanical energy generated from ball milling to produce a piezoelectric electrochemical effect.[134] Meanwhile, in conjunction with the mechanochemical effect produced by ball milling, toluene is oxidized to phenol in an air atmosphere. The mechanism of this process is primarily due to the oxygen in the air and the superoxide radicals ($^{\bullet}O_2^{-}$) generated by the piezoelectric effect of BSS being the main oxidants for the oxidation of toluene. With an oxidation potential of −0.33 V relative to NHE, $^{\bullet}O_2^{-}$ is capable of oxidizing toluene to phenol without over-oxidation.

Beyond the aforementioned methods, oxidation of functional groups can also be catalyzed by peroxidase enzymes. Yoon's research is primarily based on oxidation functionalization reactions catalyzed by peroxidases, which are catalyzed by

H_2O_2 generated through piezocatalysis.[132] By utilizing the piezocatalytic properties of bismuth oxychloride (BiOCl), H_2O_2 is continuously provided, driving biocatalytic oxyfunctionalization reactions (Fig. 7k). In this study, mechanical energy (ultrasound-driven) is used as the form of energy to drive peroxidase reactions in a much simpler way than other existing methods.

Similarly, Chen et al. also utilized ultrasound to drive the selective oxidation of 5-hydroxymethylfurfural (HMF) into 5-formyl-2-furancarboxylic acid (FFCA).[135] Hydroxyapatite decorated with platinum (Pt/HAP) is used for the piezocatalytic oxidation of HMF. The introduction of platinum leads to the creation of an interfacial electric field. The combination of the non-local piezoelectric field and the localized interfacial electric field greatly enhances the transfer of both bulk and surface charges. Furthermore, platinum not only promotes the separation of piezo-induced charges but also activates oxygen molecules and the organic functional groups of the substrates. Compared to the original hydroxyapatite, Pt/HAP exhibits outstanding piezocatalytic activity, achieving a 96% conversion rate of HMF and a 70% yield of FFCA within 2 hours at room temperature. Various aldehydes and alcohols, such as fatty aldehydes, furan aldehydes, fatty alcohols, and ethylene glycol, are universally oxidized into carboxylic acids by this catalyst. It can be said that piezocatalytic technology offers a new method for biomass conversion.

Furthermore, in addition to the previously mentioned synthesis of C1–C2 chemicals using carbon dioxide as feedstock, utilizing methane as feedstock for value enhancement through piezocatalysis is also a promising strategy for the production of high-value C1+ chemicals. Zhou and colleagues used hydroxyapatite as a piezocatalyst for methane conversion, obtaining alcohol as the liquid product, with no traces of CO or CO_2 in the products.[136] Under ultrasonic vibration, reactive oxygen species (ROS) are generated, among which $^{\bullet}OH$ attacks the C–H bonds of light alkanes, thereby producing the corresponding alcohols. Due to the negative surface charge (SC) induced by ultrasonic vibration on hydroxyapatite, methanol dehydration occurs, producing methyl carbene, which converts methanol into ethanol and ethanol into 2-propanol. When the ratio of methane to O_2 is 1 : 0.5, the efficiency of methane conversion via piezocatalysis using hydroxyapatite reaches its peak, with the production rates of methanol, ethanol, and 2-propanol being 84.4, 43.2, and 9.6 μmol g^{-1} h^{-1}, respectively. Simultaneously, radical coupling and methyl carbene-assisted C–C bond formation promote the product upgradation to larger alcohols and even multi-carbon compounds, rather than leading to over-oxidation. After methanol conversion, several C4 and C5 products are identified, including ketones (2-butanone, 2-pentanone, and 3-pentanone) and esters (methyl propionate and methyl butanoate), and even a C6 product (1,1-diethoxyethane) is discovered following ethanol conversion. The degree of carbon chain growth can be controlled based on the duration of ultrasonic treatment. In summary, piezocatalytic technology provides a novel approach for the production of multi-carbon chemicals.

4. Piezo-photocatalysis for value-added chemical synthesis

Photocatalytic synthesis of chemicals is a technology that uses light energy to excite electrons on the surface of a catalyst to carry out chemical reactions.[137] Compared to traditional catalytic reactions, photocatalytic synthesis requires clean, renewable solar energy as a power source, offering higher energy efficiency and reducing the exploitation and use of fossil fuels. Since photocatalytic synthesis can be conducted with specific photocatalyst materials, it avoids the production of by-products and increases the purity of the target product.[138] Piezo-photocatalysis is a novel method that introduces a piezoelectric field into photocatalytic reactions.[139] As mentioned earlier, piezo-photocatalysis based on piezoelectric semiconductor catalytic materials leads to modulation of the band structure due to the introduction of a piezoelectric field, thereby enhancing charge transfer. Furthermore, for the production of chemicals, the piezoelectric polarization field can also facilitate the transfer of reactants, products, and intermediates, thereby accelerating the reaction rate and improving catalytic efficiency.[140] By adjusting the intensity and frequency of the piezoelectric field, the conditions for piezo-photocatalytic synthesis of chemicals can be precisely controlled, thereby optimizing the reaction rate.[139] In summary, the enhanced catalytic activity and mass transfer effects make piezo-photocatalysis more efficient in chemical synthesis compared to photocatalysis.

Since piezo-photocatalysis is essentially based on piezoelectric semiconductor materials, the development of synthesizing value-added chemicals through piezo-photocatalytic technology also relies on existing piezoelectric semiconductor catalysts. These piezoelectric semiconductor catalysts need to possess both piezoelectric properties and excellent photocatalytic characteristics. This section details the compositions and advancements in piezoelectric semiconductor catalysts for the synthesis of value-added chemicals.

4.1 Perovskite metal oxides

Currently, among various photocatalyst materials, perovskite oxides (with the general formula $A_xB_yO_z$) have become significant semiconductor photocatalysts due to their highly stable properties and structural flexibility.[141] Simultaneously, some of these perovskite semiconductors also exhibit notable piezoelectric properties, making these specific perovskites suitable as piezo-photocatalysts for the synthesis of value-added chemicals.

In the semiconductor photocatalytic CO_2 reduction reaction, the position of the semiconductor conduction band (CB) must meet the reduction potential of CO_2 for the reaction to occur. However, the conduction band minimum of most perovskite oxides does not satisfy the reduction potential of carbon dioxide (CO_2). He *et al.* employed a piezoelectric polarization method to overcome the inherent redox potential limitations of perovskite photocatalysts. Using traditional flake-shaped $BiFeO_3$ (BFO) as a catalyst, which possesses piezoelectricity, it can collect mechanical energy, thereby generating piezoelectric

polarization. This process consequently modulates the band structure, breaking the limitations of perovskite oxide photocatalysts in the photoreduction of CO_2 (Fig. 8a).[142] Under the action of ultrasonic vibration stress, it generates a large amount of free polarized charges. These polarized electrons on the surface of BFO trigger various piezoelectric oxidation–reduction reactions, promoting the piezocatalytic conversion of carbon dioxide (CO_2) to methane (CH_4) (Fig. 8b). This method mainly adjusts the band structure of BFO, engineering its electronic states to meet the reduction potential of CO_2. At the same time, by changing the length of the Fe–O bond, it enhances the conductivity and piezoelectric charge separation efficiency during the reaction. This process aids in alleviating the rate-limiting steps formed by $^\bullet COOH$ and $^\bullet CH_3OH$, enhancing CO_2 adsorption capability, and lowering the energy barrier for the CO_2 reduction reaction.

In the photocatalytic process, the rapid recombination of photogenerated electrons and holes has always been one of the major obstacles in photocatalysis.[143] Therefore, piezo-photocatalysts generally utilize ultrasonic radiation, mechanical stirring, or ball milling to create a piezoelectric potential inside the nanocrystals, facilitating the separation of photogenerated electrons and holes. Differing from previous studies, Wang *et al.* employed a low-power ultraviolet pulsed laser (PL) (3 W, 355 nm) as the UV light source. Without the need for external mechanical contact, they are able to enhance the efficiency of carbon dioxide reduction using the piezoelectric photocatalyst $BaTiO_3$ (BTO-T), demonstrating exceptional performance.[144] This is mainly because the enormous transient photonic pressure of the 355 nm PL (5.7×10^7 Pa, 2.7 W) not only bends the energy bands of BTO-T to meet the reduction potential of carbon dioxide but also induces a pulsed internal electric field, effectively separating photogenerated carriers. Building on this, the PL-triggered piezo-photocatalytic reduction of CO_2 achieved the highest performance reported, with a CO yield reaching 52.9 mmol g^{-1} h^{-1} at the millimolar level, thus realizing efficient photocatalytic reduction of CO_2 (Fig. 8c and d).

In the process of enhancing the performance of perovskite metal oxides, the introduction of controllable defects is also a main direction of research. Yuan *et al.* utilized defects and piezoelectricity to improve the activity of the piezo-photocatalytic nitrogen reduction reaction (NRR) and revealed the synergistic catalytic mechanism of $BaTiO_3$ with adjustable oxygen vacancies (OVs).[145] The introduced oxygen vacancies altered the piezoelectric polarization of $BaTiO_3$, effectively enhancing the separation efficiency of photogenerated carriers. Using the aforementioned method, $BaTiO_3$ with moderate OVs achieved a piezo-photocatalytic NH_3 release efficiency of 106.7 μmol g^{-1} h^{-1}, far surpassing the catalytic performance of previous piezocatalysts or piezo-photocatalysts. Besides controllable defect tuning, doping with metal elements is also one of the main research directions for improving the performance of piezoelectric catalysts. In the piezocatalytic reaction for producing hydrogen peroxide, Zhou *et al.* utilized niobium-doped tetragonal $BaTiO_3$ ($BaTiO_3$:Nb) sensitized with carbon

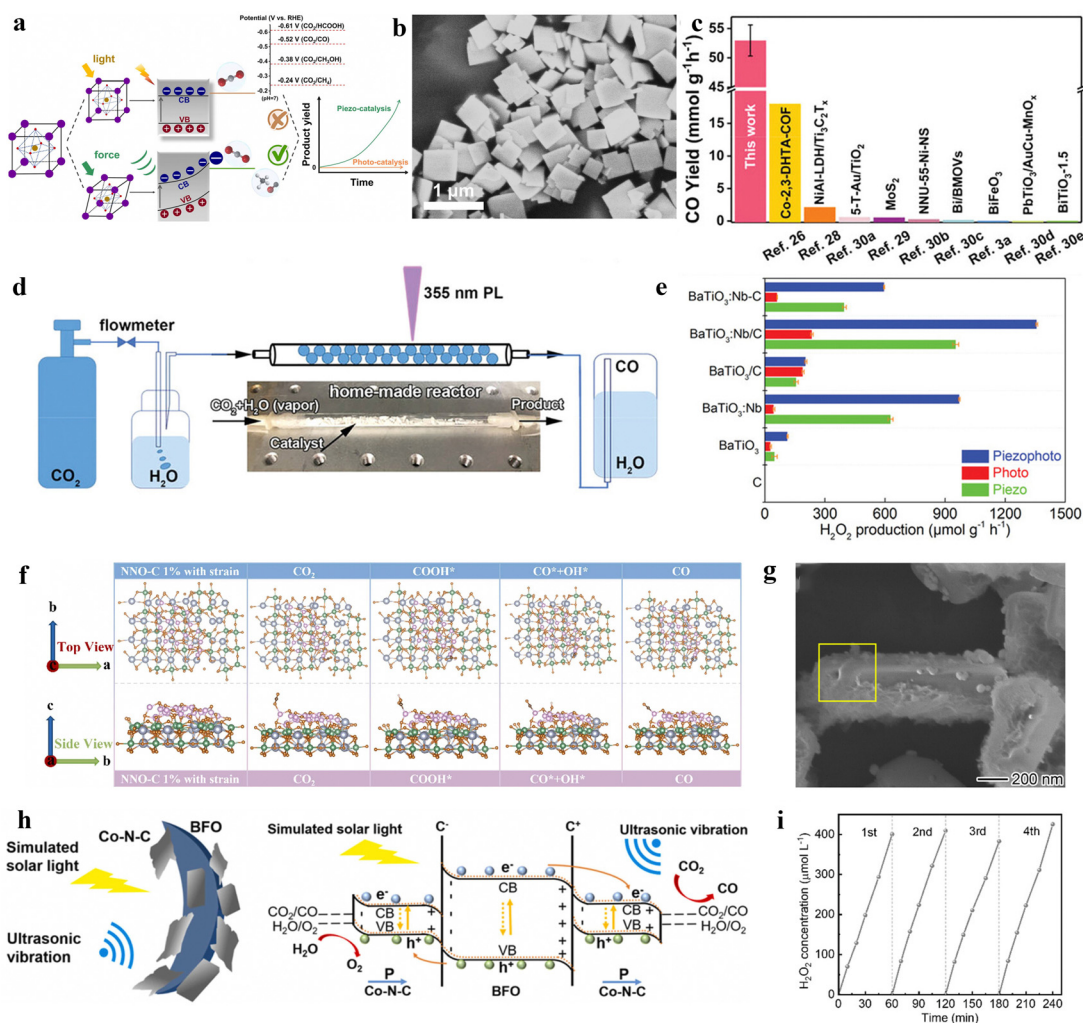© 2024 The Author(s). Published by the Royal Society of Chemistry

Fig. 8 (a) Concept of the photo and piezoelectric-catalytic CO_2 reduction pathway with perovskite oxide piezoelectric materials. (b) SEM image together with the corresponding elemental mappings of BFO nanosheets.[141] Copyright 2022 Elsevier B.V. (c) The comparison of CO yields among the laser-catalytic CO_2 reduction in this work and reported photocatalysts and piezoelectric photocatalysts. (d) Schematic diagram.[144] Copyright 2023 Wiley-VCH GmbH. (e) Comparison of the H_2O_2 production rates with various catalysts in piezo-, photo-, and piezophoto-catalytic reactions. C denotes preparations with carbon quantum dots, /C in nanorod-like nanoparticles, and −C in spherical nanoparticles.[146] Copyright 2022 Wiley-VCH GmbH. (f) The optimized geometric structures in the reaction path for NNO-C 1% with strain.[147] Copyright 2023 Elsevier B.V. (g) Detailed composition analysis of AuCu/PbTiO₃/Mnox: EDX spectra of the selective area in the SEM image.[148] Copyright 2023 American Chemical Society. (h) Diagrammatic sketch for the piezo-photocatalytic mechanism of the Co−N−C@BFO heterostructures.[149] Copyright 2023 Elsevier B.V. (i) Catalytic stability tests.[150] Copyright 2022 Wiley-VCH GmbH.

quantum dots (CDs).[146] The photosensitizer excites electrons into the semiconductor's conduction band, while the piezoelectric polarization directs the electrons to the semiconductor surface, significantly enhancing the efficiency of hydrogen peroxide production. The use of the piezoelectric polarization field limited the recombination process of photogenerated electrons and holes. Under the combined action of visible light and ultrasound, the yield of hydrogen peroxide (H_2O_2) is 1360 μmol g⁻¹ h⁻¹. This proved that CDs can enhance the piezocatalytic activity of BaTiO₃:Nb. It is demonstrated that piezo-photocatalysis surpasses the yield of either sole photo-catalysis or piezocatalysis (Fig. 8e). This phenomenon can be attributed to the piezoelectric response of BaTiO₃, which increases the production rate. In this work, it is confirmed that

BaTiO₃:Nb/C induced the highest H_2O_2 generation rate, and modification of both nanorod-like particles and CDs could enhance the generation rate.

In addition to utilizing defects and metal modifications in piezoelectric catalyst materials, using metal oxides to modify piezoelectric catalysts for carbon dioxide reduction has also become one of the methods to solve the rapid recombination process of photogenerated electron–hole pairs. Wang *et al.* introduced cobalt oxide (Co₃O₄) into nano-sized NaNbO₃ using a direct photo-deposition method, causing distortion in the NbO₆ octahedra (Fig. 8f).[147] This alteration changes the symmetry of nano NaNbO₃, thereby enhancing its piezoelectric performance. Simultaneously, the increase in Co sites facilitates the adsorption of carbon dioxide, reducing the reaction

barrier. The results showed that under the modification of CO_3O_4, nano $NaNbO_3$ cubes exhibit excellent carbon dioxide reduction performance under the synergistic action of ultrasound and visible light, with a CO yield of about 4579.71 μmol g^{-1} h^{-1} during the reaction process. Ultimately, pure NNO exhibited the lowest photocatalytic CO and CH_4 yield, with the highest rates of carbon monoxide and methane production at 1% NNO-C.

Due to poor charge recombination and slow surface reactions in photocatalytic and piezoelectric catalytic processes, which hinder practical applications, Yang and colleagues proposed a dual co-catalyst strategy to enhance piezoelectric catalytic performance.[148] AuCu reduction and MnO_x oxidation co-catalysts were deposited on the opposite polar surfaces of $PbTiO_3$ nanosheets (Fig. 8g). This reaction creates an embedded electric field at the interface between the semiconductor and the co-catalysts, resulting in a band bending electric field. This electric field, combined with the inherent ferroelectric field, piezoelectric polarization field, and band bending within the $PbTiO_3$ bulk, strongly drives the generated electrons to migrate towards AuCu and MnO_x, thereby preventing the rapid recombination of photogenerated electrons and holes that leads to decreased yield. AuCu/$PbTiO_3$/MnO_x significantly improved charge separation efficiency and notably enhanced the piezo-photocatalytic activity for CO and O_2 generation. This strategy offers a new way to better couple photocatalysis and piezocatalysis, promoting the transformation of CO_2 and H_2O.

Based on past research showing that the synergistic effects of novel piezoelectric catalysts and traditional photocatalysts can significantly improve catalytic performance, Xu *et al.* designed a heterostructured piezo-photocatalyst comprising Co–N–C and $BiFeO_3$ (BFO) for the piezo-photocatalytic reduction of carbon dioxide (Fig. 8h).[149] In the piezo-photocatalytic reaction process, an internal electric field promotes the transfer of electrons to the active sites of Co–N–C. The presence of electrons promotes the two-electron carbon dioxide reduction process. Additionally, in the energy band of BFO, the transfer of electrons to Co–N–C is also enhanced, participating in the carbon dioxide reduction process. Under the catalytic action of the Co–N–C@BFO(1:7) catalyst, the reduction of carbon dioxide to CO and CH_4 significantly increases, with yields of 1373.41 μmol g^{-1} and 169.32 μmol g^{-1} respectively, markedly enhancing the photocatalytic performance of carbon dioxide reduction.

In addition to enhancing the catalytic performance of piezo-photocatalysts through the combination of two materials, the use of surface doping and self-assembly to prepare a more compact nano-composite material can also improve the catalytic performance of piezoelectric photocatalysts. Zhang and colleagues reported an ultra-compact nano-composite material ($LaFeO_3$/$ZnFe_2O_4$/La_2O_3) induced by a facial dopant-induced self-assembling strategy.[150] This composite material is synthesized at 800 °C through a one-pot method, thereby creating self-assembled interfaces during the multiphase formation process, and inducing autonomous assembly processes for compositional optimization through surface zinc addition.

The introduced zinc forms spinel-like $ZnFe_2O_4$, ensuring close contact between the semiconductor $LaFeO_3$ and the piezoelectric $ZnFe_2O_4$/La_2O_3 phases, which enhances the piezoelectric properties and electrical resistance of the hybrid material. In this composite, the synergistic effect of oxygen activation is enhanced by manipulating photogenerated electrons and the piezoelectric effect produced by vibrations, thus increasing the efficiency of piezo-photocatalytic production of hydrogen peroxide. LFZ-0.3 exhibits excellent piezo-photocatalytic activity and stability under 30% Zn conditions (Fig. 8i).

4.2 Carbon nitride

The development of broad-spectrum responsive photocatalysts is an important avenue for enhancing photocatalytic efficiency.[37,151] Among them, graphitic carbon nitride (g-C_3N_4) is a typical visible light-responsive semiconductor photocatalytic material, which also possesses piezoelectric properties. The advantages of carbon nitride, such as the earth abundance of its constituent elements, stable physicochemical properties, tunable surface structures, and suitable band gap positions, are also applicable in the field of piezo-photocatalysis. Therefore, carbon nitride-based catalysts, as piezoelectric semiconductor materials with numerous advantages, hold significant practical importance for the piezo-photocatalytic production of chemicals. However, the piezoelectricity of carbon nitride is limited by its symmetrical structure, requiring ultra-thin nanosheets, and it also suffers from quick recombination of photo-generated charges and a lack of active sites. Therefore, further modification is often required in practical applications. Song *et al.* developed a molecularly embedded carbon nitride using a copolymerization method, embedding benzene-1,4-dicarboxylic acid dihydrazide units in diaminotriazine cyanoresin (DKCN). The sample prepared in this way demonstrated excellent catalytic performance in the photocatalytic nitrogen reduction process (Fig. 9a).[152] It is demonstrated that the introduction of linkers and D–A (donor–acceptor) units (Fig. 9b) redistributed the distribution of charge centers, thereby expanding the in-plane polarization of C_3N_4. This significantly enhanced the separation of photo-induced carriers, providing active sites for photocatalysis. Additionally, the large built-in electric field provided by the piezoelectric potential under ultrasound can cause charge polarization, thereby driving photogenerated carriers to migrate in different directions. As a result, the optimal nitrogen fixation yield of piezo-photocatalysis reached 183.3 μmol g^{-1} h^{-1}, which is 21.6 times that of the original carbon nitride material. Vuong *et al.* introduced metals on the surface of the existing g-C_3N_4 to alter the piezo-photocatalytic performance.[153] Due to defects in the material and the formation of new metal-carbon bonds, electron dissociation sites are provided for the system, facilitating the separation and migration of excited state charges. This process avoids the rapid recombination of electrons and holes. Moreover, compared to Mg and Ca, the introduction of Ba results in more negative conduction bands (CB) in the material, thereby hindering the water oxidation reaction (WOR) and reducing the production rate of hydrogen peroxide
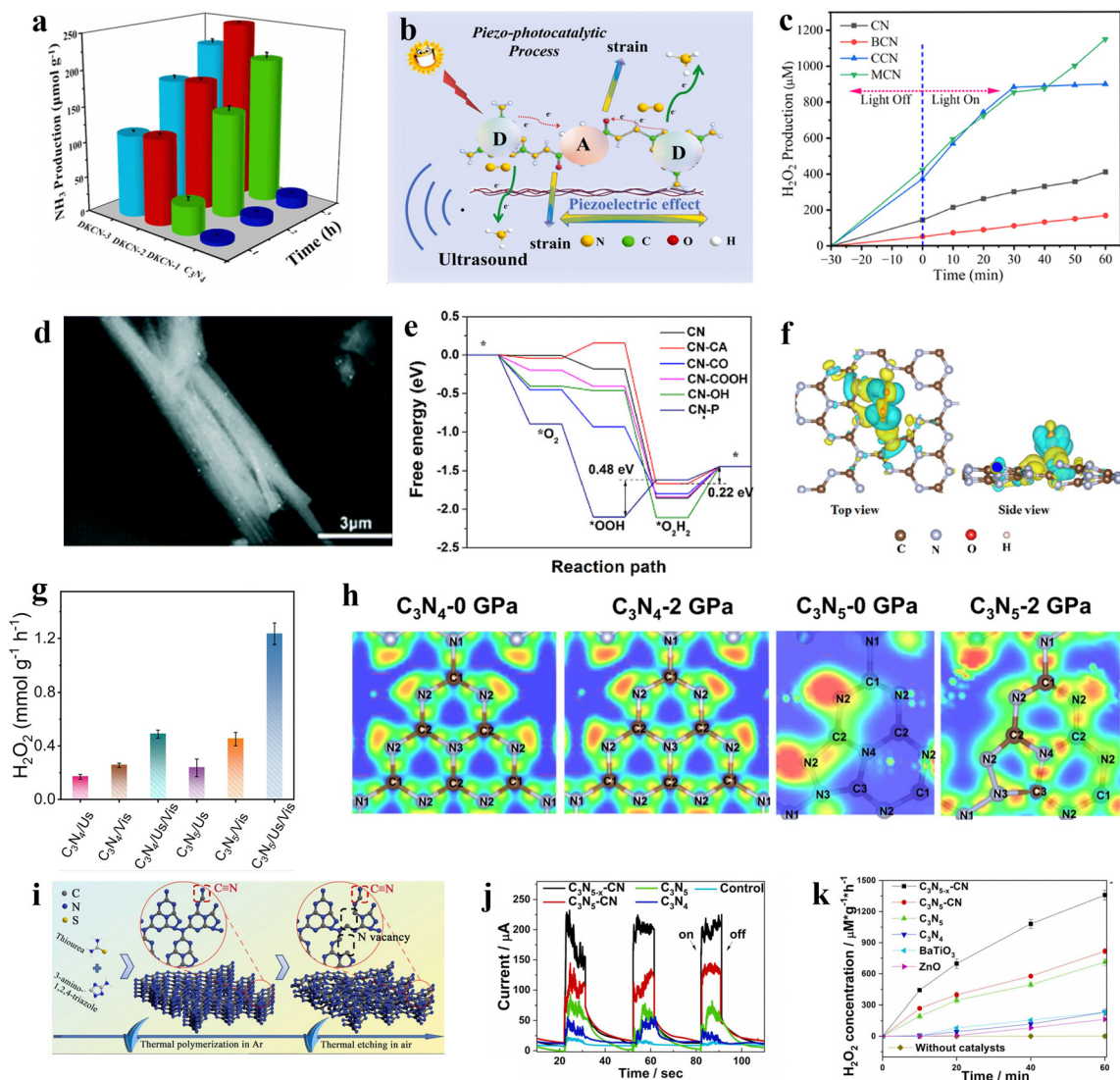
Fig. 9   (a) Catalytic performance of prepared samples in the photocatalysis nitrogen reduction reaction; (b) piezo-photocatalytic nitrogen reduction mechanism over DKCN.[152] Copyright 2023 Elsevier Ltd. (c) Piezo-photocatalytic H_2O_2 production of CN, BCN, CCN, and MCN.[153] Copyright 2023 Elsevier Ltd. (d) Schematic diagrams of deposited Au on melon, PHI and PTI. SEM images of Au deposited samples taken using the backscattered electronic pattern.[155] Copyright 2023 American Chemical Society. (e) Calculated energy profile for hydrogen peroxide production on different sites; charge density difference mapping between H_2O_2 and reaction sites. (f) CN the sky-blue and yellow isosurfaces stand for the negative and positive charges, respectively.[156] Copyright 2023 American Chemical Society. (g) Corresponding histograms of the H_2O_2 yield at 60 min. (h) Reactive sites in photocatalytic H_2O_2 production. (c) ELF with 0 and 2 GPa (isolevel = 0.8).[157] Copyright 2023, Springer Nature. (i) The synthetic route of C_3N_5-x-CN. (j) Transient current response of different systems: in the absence of the PMS. (k) Piezo-photocatalytic H_2O_2 evolution of different catalysts.[158] Copyright 2023 Elsevier B.V.

(Fig. 9c). Ultimately, the modified carbon nitride, used as a catalyst and under the enhanced effect of piezoelectric polarization combined with one hour of light irradiation, achieved a hydrogen peroxide concentration of 1147.03 μM.

Different heteroatoms can be doped into carbon nitride-based materials to enhance catalytic activity. Tran et al. prepared sulfur (S) and selenium (Se) doped g-C_3N_4, and investigated the changes in piezo-photocatalytic hydrogen peroxide production performance before and after doping.[154] Under the same conditions, Se-doped g-C_3N_4 exhibits superior catalytic performance compared to S-doped g-C_3N_4. Simultaneously,

they found that the doping precursors significantly affect the defect states of the material, with SeO_2 as the doping precursor having the most optimal enhancing effect on the performance of carbon nitride.

To investigate the impact of different structures on the performance of g-C_3N_4 piezoelectric catalytic materials, Zhang et al. conducted detailed studies on the piezoelectric properties and piezoelectric-assisted photocatalytic performance of three different structural GCNs: melon-like, polyheptazine imide (PHI), and polytriazine imide (PTI).[155] The results showed that under ultrasonic action, polytriazine imide (PTI) demonstrated

the best piezocatalytic performance in typical potassium permanganate reduction and hydrogen peroxide generation reactions. Furthermore, the morphology significantly impacts the piezoelectric performance of PTI. PTI hollow tube structures, subjected to forces, exhibit geometric anomalies on the surfaces of regular pores such as prisms, rectangles, squares, and polygons, leading to stress accumulation (Fig. 9d). However, in round, elliptical, and spherical cavities, the curved surfaces along the inner axes disperse the accumulated stress, resulting in less strain and inferior piezoelectric performance. Therefore, the different macroscopic morphologies of melon-like, PHI, and PTI carbon nitride ultimately result in diversified piezoelectric performances.

Molecular engineering modifications of carbon nitrides also lead to enhanced piezo-photocatalytic performance. Wang *et al.* conducted precise molecular structure regulation of graphitic carbon nitride (CN) to study the effect of piezoelectricity on photocatalytically generated H_2O_2 on CN.[156] They synthesized phosphorus-modified CN (CN–P), oxygen-functionalized CN (CN–OF), and cyano group (CA)-grafted CN (CN–CA) to investigate the synergy between molecular engineering and the piezoelectric effect in photocatalytic H_2O_2 production over CN. It is concluded that the piezoelectric effect in photocatalytic generation of hydrogen peroxide on CN depends on the molecular structure of CN, and the introduction of surface groups caused significant changes in the density of states (DOS) (Fig. 9e). Particularly, the electronic state of CA is located in the higher region of the conduction band (CB), indicating that electrons captured in the CA group have strong reduction capabilities (Fig. 9f). This proves that introducing P and oxygen groups on CN enhances the separation and transfer of photo-generated charges and the piezoelectric scheme, optimizing the active potential barrier for the transformation of O_2 into H_2O_2, thereby enhancing the piezoelectric effect in photocatalytic hydrogen peroxide production. Although CN–CA has the lowest energy barrier and the highest charge separation efficiency under sole light irradiation, the group adjustment of CA causes piezoelectric polarization to damage certain photogenerated carriers at active sites, ultimately leading to a decrease in piezo-photocatalytic activity.

Constructing composite materials can also enhance the performance of piezo-photocatalytic synthesis of chemicals using carbon nitride. Phan *et al.* reported an *in situ* one-step solid-state method based on the S-scheme heterojunction charge transfer mechanism, for preparing piezo-photocatalytic materials (CdS/g-C_3N_4) used in the synthesis of hydrogen peroxide.[159] This composite material exhibited a catalytic efficiency of 23.44 mmol g^{-1} h^{-1} under visible light and ultrasonic irradiation. The study demonstrated that the CdS sites could accumulate excited electrons and effectively enhance the composite material's catalytic ability to reduce oxygen (O_2) to produce hydrogen peroxide (H_2O_2). It further proved that the S-scheme heterojunction significantly strengthens the piezo-photocatalytic performance of the CdS/g-C_3N_4 composite material.

Nitrogen-rich carbon nitride (C_3N_5) is an emerging type of carbon nitride. The polymerization of the triazole and triazine frameworks to form nitrogen-rich carbon nitride leads to structural asymmetry and a resultant dipole moment due to the noncoincidence of positive and negative charge centers. This strong dipole moment implies that the dipole field-driven spontaneous polarization in C_3N_5 can be harnessed to utilize photogenerated charge separation kinetics. Therefore, it generally possesses superior piezocatalytic properties compared to the classic g-C_3N_4. This has been confirmed in the work of Li and colleague, where C_3N_5 demonstrated the most exceptional piezo-photocatalytic efficiency for the generation of hydrogen peroxide (Fig. 9g).[157] The electron cloud in both samples without pressure is smaller than in the sample under pressure (Fig. 9h). Notably, the active charge distribution in C_3N_4 remains almost unchanged, while in C_3N_5, it shifts from the left N_2 position to the right N_2 and N_4 positions, from 0 to 2 GPa. This phenomenon indicates that the introduction of the triazole ring causes asymmetry, promoting the change of polarized sites with pressure. This new process utilizes photoinduced charge dynamics to produce hydrogen peroxide. Under simulated sunlight and ultrasonic waves, C_3N_5 demonstrated a high rate of hydrogen peroxide photosynthesis and excellent charge transfer selectivity (92% $2e^-$ transfer). This achievement is attributed to the introduction of nitrogen-rich triazole rings in C_3N_5, which not only generated a dipole field but also induced a spontaneous polarization field, accelerating targeted electron transfer at active nitrogen sites. This process promotes the production of hydrogen peroxide through an indirect $2e^-$ transfer pathway (Pauling-type adsorption). This innovative method of controlling photogenerated carrier migration and transport with a dipole field opens new avenues for enhancing photosynthesis efficiency through structural engineering. Fu *et al.* further introduced dual defects into the C_3N_5 piezoelectric semiconductor material.[158] They synthesized a piezoelectric photocatalyst of semiconductor C_3N_5 with –CN substitution and nitrogen vacancies, by employing a two-step thermal polymerization and thermal etching process (Fig. 9i). This piezoelectric catalyst (C_3N_5-*x*-CN) with dual defect sites achieved a synergistic enhancement of piezoelectric and photoelectric properties in the ultrasonic-assisted photocatalytic system (Fig. 9j). Experimental data on hydrogen peroxide evolution in different catalysts under piezo-photocatalytic conditions (Fig. 9k) confirmed that C_3N_5-*x*-CN, being more porous and thinner than C_3N_5–CN, is more conducive to enhanced polarization. In summary, due to defect engineering creating an active catalytic surface that increases piezoelectricity and promotes carrier separation, the catalyst's light absorption is enhanced, achieving higher piezo-photocatalytic efficiency.

4.3 Bismuth-based materials

Bismuth-based photocatalysts, with their narrow band gap resulting from the hybridized orbitals of Bi 6s and O 2p in the valence band, are well-suited for visible light-driven photocatalysis.[160] Therefore, when bismuth-based materials are used as piezo-photocatalysts, they exhibit a broader range of light absorption compared to metal oxide piezocatalytic materials, and possess a comparable level of stability. Of

course, unlike the relatively fixed band positions of carbon nitrides, the band structures of different bismuth-based materials vary significantly, hence the catalytic reactions they are used for also differ.[160,161] Leveraging the advantages of bismuth-based materials, Tu and colleague reported a piezoelectric catalyst material, $Bi_4W_{0.5}Ti_{0.5}O_8Cl$, in which tungsten (W) and titanium (Ti) co-occupy the B-site of the perovskite layer.[162] The crystal structure of $Bi_4W_{0.5}Ti_{0.5}O_8Cl$ viewed from different orientations shows that atoms aligned along the a and c axes exhibit a high degree of central symmetry. However, when viewed from the *a–c* plane, the crystal structure is non-centrosymmetric. Additionally, due to the growth of $Bi_4W_{0.5}Ti_{0.5}O_8Cl$, the material accumulates polarity along the *b*-axis direction (Fig. 10a). This non-centrosymmetric structure of $Bi_4W_{0.5}Ti_{0.5}O_8Cl$ endows the catalyst material with excellent piezoelectric catalytic properties. The results indicate that the hydrogen peroxide (H_2O_2) yield can reach as high as 530.4 μmol h^{-1} g^{-1} in the absence of metal deposition on the $Bi_4W_{0.5}Ti_{0.5}O_8Cl$ catalyst (Fig. 10b). Due to the enhanced piezo-photocatalytic kinetics and thermodynamics, combined with the advantages of bismuth-based materials, the generation of

hydroxyl radicals (•OH) and hydrogen peroxide is significantly promoted.

In photocatalytic processes, the use of noble metal loadings often rapidly enhances the rate of charge migration, while also providing more active sites for catalytic reactions. This method is equally effective under the influence of a coupled piezo-electric polarization field. Chen *et al.* prepared Bi_5O_7I nanorods using a simple solvothermal calcination method and for the first time applied them in piezoelectric/photocatalytic nitrogen fixation and the degradation of methyl orange (MO).[163] To further enhance the catalytic activity of Bi_5O_7I, metallic silver nanoparticles are used as co-catalysts to modify it (Fig. 10d). The addition of Ag significantly increased the photocurrent under simulated sunlight irradiation. However, as the Ag content increased, the photocurrent of the Ag/Bi_5O_7I electrode first increased and then decreased. Compared with other samples, the 2.5% Ag/Bi_5O_7I photocatalyst exhibited the highest photo-current (Fig. 10c), which is 2.5 times higher than that of pure Bi_5O_7I. The results indicate that the prepared Ag/Bi_5O_7I demonstrates excellent piezo-photocatalytic performance in photo-catalytic nitrogen fixation under light/piezoelectric conditions.

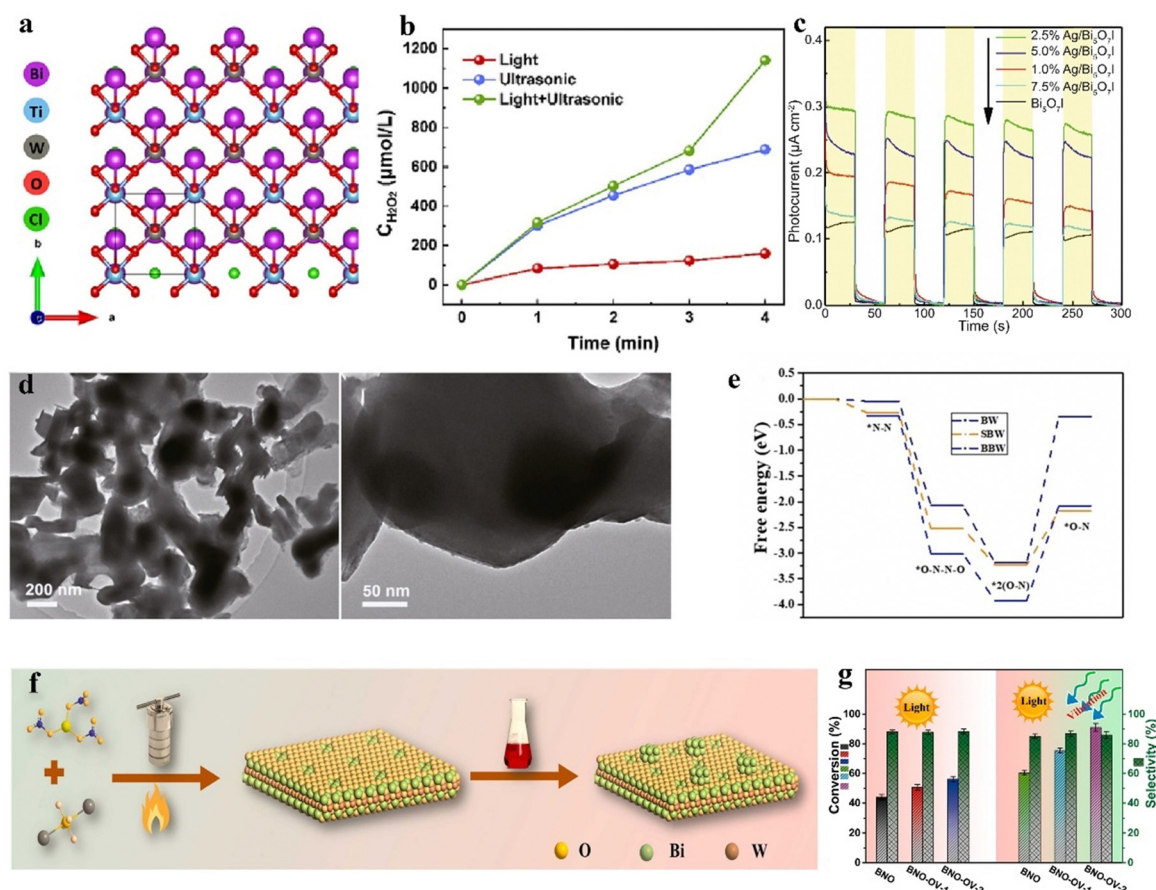Fig. 10 (a) Crystal structure in the *a–b* plane of $Bi_4W_{0.5}Ti_{0.5}O_8Cl$. (b) H_2O_2 concentration as a function of reaction time.[162] Copyright 2023 Elsevier B.V. (c) Transient photocurrent response of Bi_5O_7I and Ag/Bi_5O_7I with different Ag contents. (d) TEM images of 2.5% Ag/Bi_5O_7I.[163] Copyright 2021 Institute of Process Engineering, Chinese Academy of Sciences. (e) Gibbs free energy for the nitrogen oxidation to nitric acid progress over BBW.[164] Copyright 2023 Elsevier B.V. (f) Schematic of the synthesis method. (g) Catalytic activity of various catalysts in the aerobic coupling of benzylamine under light irradiation (left) or light irradiation coupling with vibration (right).[165] Copyright 2021 Elsevier Ltd.

Besides the production of hydrogen peroxide and ammonia which requires the piezo-photocatalytic action of bismuth-based materials, the synthesis of essential chemicals like nitric acid can also adopt this approach.[166] Nitric acid is an essential chemical for agriculture and industry. The current industrial production primarily relies on the Ostwald process.[167] However, its high energy consumption and carbon emissions have led people to seek new, milder methods for synthesizing nitric acid. Deng and colleagues utilized the piezoelectric polarization effect of Bi_2WO_6-based catalysts to achieve the synthesis of nitric acid at room temperature.[164] The effective utilization of piezoelectrically induced charges is a primary direction for enhancing the process. Introducing the tip effect and structural disorder of Bi_2WO_6 to set up a qualitative electric field is also one of the methods to improve efficiency. The tip effect can form the main strain and potential centers for clusters and vacancies, thereby strengthening the piezoelectric polarization electric field and the internally built electric field from the light in the same direction, which in turn promotes charge transfer and charge dissociation. Furthermore, the presence of clusters and vacancies as activation sites for oxygen and nitrogen can reduce the surface resistance of the reaction (Fig. 10e). Also, in

the absence of a co-catalyst, Bi_2WO_6 enriched with Bi and O vacancies exhibits a good rate of piezo-photocatalytic nitrogen oxidation for synthesizing nitric acid (5.26 mg g^{-1} h^{-1}), which is five times that of pure Bi_2WO_6.

N-Benzylidenebenzylamine is widely used in the synthesis of pharmaceuticals and bioactive compounds; therefore, the mild synthesis of N-benzylidenebenzylamine from benzylamine through selective oxidation via C–N coupling is an important synthetic approach. Wang et al. synthesized Bi_4NbO_8Br nanosheets oriented along the [001] direction with oxygen vacancies. Specifically, through the flux method and H_2/Ar heat treatment, Bi_4NbO_8Br nanosheets (BNO) oriented in a specific direction and rich in oxygen vacancies are synthesized (Fig. 10f).[165] The synergistic effect of vibration-induced electric fields and oxygen vacancies can improve the selectivity of the reaction. Under the simultaneous action of light irradiation and mechanical vibration, the aniline conversion rate of oxygen-vacancy-rich BNO-ov-2 is 2.1 times that of the original BNO under light irradiation alone. Electrochemical results indicated that under the piezoelectric field induced by vibration, it is conducive for the separation and transfer of photogenerated electrons and holes from the bulk to the surface, and
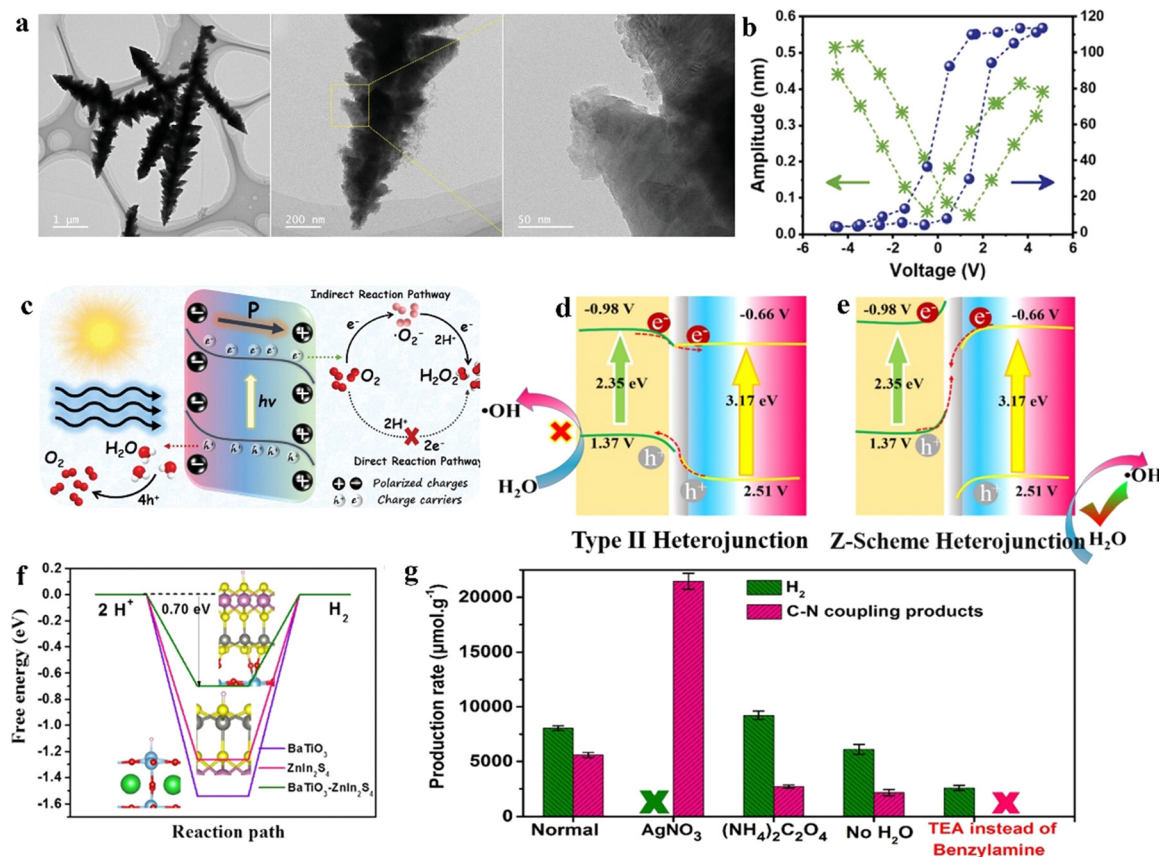

Fig. 11 (a) $Cd_{0.5}Zn_{0.5}S$ TEM image; (b) local piezoelectric butterfly curve and phase hysteresis loop of $Cd_{0.5}Zn_{0.5}S$; (c) schematic mechanism of the probable H_2O_2 evolution pathway over $Cd_{0.5}Zn_{0.5}S$ in piezocatalysis and photocatalysis.[168] Copyright 2022 Wiley-VCH GmbH. (d) Schematics of a type II heterojunction system and (e) the schematics of the Z-scheme system for $BaTiO_3$@$ZnIn_2S_4$. (f) Schematic diagram of the dehydrogenation and C–N coupling of benzylamine on $BaTiO_3$–$ZnIn_2S_4$. (g) Catalytic activity of $BaTiO_3$@$ZnIn_2S_4$ under various reaction conditions exposed full-spectrum light irradiation coupling with vibration.[169] Copyright 2021 Elsevier Ltd.

the presence of oxygen vacancies further inhibits their recombination on the catalyst surface (Fig. 10g). The synergistic effect of the piezoelectric effect and oxygen vacancies facilitated the selective oxidation of aniline to N-benzylideneaniline under photocatalytic conditions. By combining the unique advantages of bismuth-based materials with the appropriate incorporation of oxygen vacancies, the rates of piezo-photocatalytic N-benzylidenebenzylamine production can be further enhanced.

4.4 Transition metal sulfide

In addition to the aforementioned metal oxides, carbon nitrides, and bismuth-based materials, transition metal sulfides, as emerging piezoelectric semiconductor materials, are receiving increasing attention.[170] Besides their narrow band gap and tunable band structure enabling efficient solar light absorption, their typically abundant defect structures also make them highly suitable as piezo-photocatalysts.[171,172] Based on these excellent properties, Lin et al. developed a highly efficient transition metal sulfide catalyst material for the production of H_2O_2, that is, $Cd_xZn_{1-x}S$ nanobranches (Fig. 11a).[168] This $Cd_xZn_{1-x}S$ catalyst material showed a higher rate of piezo-photocatalytic hydrogen peroxide production under ultrasonic conditions compared to the original ZnS and CdS. Without the addition of any sacrificial agents, the optimum yield of $Cd_{0.5}Zn_{0.5}S$ reached 21.9 $\mu mol\ g^{-1}\ h^{-1}$, and under visible light irradiation, its evolution rate increased to 151.6 $\mu mol\ g^{-1}\ h^{-1}$. The combination of the advantages of nanostructures and the piezoelectric properties of the prepared materials, which exhibit significant polarization switching behavior (Fig. 11b), suggests a new approach for researching piezoelectric photocatalyst materials using the effective utilization of transition metal sulfides combined with nanostructures (Fig. 11c).

Z-scheme heterojunction photocatalysts possess unique photocatalytic properties, such as a large interface contact area, rapid Z-scheme charge transfer channels, efficient photogenerated carrier separation, and maximal redox abilities.[169] Under the influence of piezoelectric polarization, the polarization field can retain and further enhance these advantages of the Z-scheme heterojunction. Wang and colleagues utilized the advantages of the piezoelectric effect and the layered Z-scheme heterostructure to construct a layered piezoelectric Z-scheme $BaTiO_3@ZnIn_2S_4$ heterostructure without the need for a co-catalyst. The Z-scheme electron transfer pathway maintains the strong redox ability of photogenerated electrons and holes and provides spatial separation of carriers and surface redox areas. Compared to pure $BaTiO_3$ or $ZnIn_2S_4$, the well-designed redox zones in $BaTiO_3@ZnIn_2S_4$ exhibit the lowest energy barriers for hydrogen production and C–N coupling (Fig. 11d and e). Moreover, the piezoelectric effect further accelerates the separation and transfer of photogenerated carriers in this structure (Fig. 11f). Utilizing the combined advantages of the piezoelectric effect and Z-scheme heterostructure, the performance of piezocatalysts is greatly enhanced under conditions of full-spectrum illumination and vibration (Fig. 11g). This work achieved high photocatalytic activities for the coupling product of C–N (N-benzylidenebenzylamine) (5593 $\mu mol\ g^{-1}\ h^{-1}$) and H_2 (8041 $\mu mol\ g^{-1}\ h^{-1}$).

5. Summary and outlook

Efficient renewable energy conversion (mechanical and light energy) through piezo-(photo)catalytic technology based on piezotronics and piezo-phototronics provides a practical path for accelerating diversified energy supply and addressing environmental pollution issues. Particularly, by utilizing green methods for the high-value transformation of chemicals, efficient and high-value utilization of existing resources can be achieved, thereby meeting the growing market demand while simultaneously contributing to environmental protection.

In the synthesis of chemicals through piezocatalytic methods, it is considered that the theoretical efficiency of electromechanical conversion is much higher than that of photoelectric conversion, this makes piezocatalytic technology potentially more applicable in the industrial sector compared to photocatalysis. Moreover, piezocatalytic technology also possesses key advantages of photocatalytic chemical synthesis techniques, such as utilizing renewable energy, having green reaction processes, producing fewer byproducts, and involving simpler synthesis procedures, among others. Simultaneously, as mentioned earlier, the fundamental mechanism of piezocatalysis is actually still debatable, with both band theory and the shielding charge effect receiving considerable support. Moreover, many current studies use ultrasound as the driving force for piezocatalytic reactions, where the associated sonochemical effects also hinder the exploration of the mechanism. However, the recent work reported by Ma et al. has provided breakthrough guidance for the understanding of the mechanism, suggesting that piezocatalytic materials with a narrow band gap may not follow the band theory. Their choice of carbon dioxide reduction reaction has played an important role in providing a clear understanding of the mechanism. That is, using certain reactions for the piezocatalytic synthesis of value-added chemicals as probe reactions may provide a clearer identification of the piezocatalytic mechanisms followed by the materials.

For piezo-photocatalytic technology in synthesizing value-added chemicals, it retains all the advantages of photocatalytic chemical production. Additionally, the band structure and charge transfer rate of piezoelectric semiconductors are enhanced due to piezoelectric polarization. As summarized in this review, the electric field established by piezoelectric polarization can significantly promote the separation and transfer of charge carriers, thereby rapidly enhancing the efficiency of chemical synthesis. Simultaneously, the modulation of the band structure not only promotes charge migration but also enhances the redox capability of piezoelectric semiconductors. This means that photocatalysts, which were previously unable to react due to unsuitable band structures, can now undergo chemical reactions under the influence of piezoelectric polarization. This significantly broadens the types of catalysts applicable to various reactions.

Although piezo-(photo)catalytic technology has quite a few irreplaceable advantages, it also faces significant challenges.

(I) The form of mechanical energy driving piezoelectric polarization. According to the summary of this review, most current piezo-(photo)catalytic reactions are driven by small-scale ultrasonic devices in laboratories. However, to achieve large-scale chemical production using piezoelectric technology, the first issue that needs to be addressed is the problem of driving stress. Large-scale ultrasonic technology may require considerable energy consumption, and the economic issues it faces need further investigation. Alternatively, there is a need to develop the use of non-ultrasonic cavitation stress or utilize natural mechanical stress available in the environment. This may be a key issue facing the future of piezoelectric (photo)catalytic technology.

(II) Novel piezo-(photo)catalytic materials. In fact, the piezo-catalysts currently developed for use in chemical synthesis are still insufficient compared to the multitude of piezoelectric materials available. In recent years, some novel piezoelectric materials, such as MXenes and graphene, have gradually emerged in the field of piezocatalysis. These novel piezocatalytic materials actually also possess potential for application in the field of chemical synthesis. Especially, some materials may have unique selectivity for organic synthesis reactions. Therefore, in the future, it will be necessary to develop and utilize more novel piezoelectric materials in the synthesis of value-added chemicals.

(III) The piezoelectric and catalytic properties of piezo-(photo)catalysts. If efficient synthesis of value-added chemicals through piezoelectric (photo)catalytic technology is desired, the piezoelectric material used as a catalyst needs not only to possess piezoelectric properties but also to have excellent catalytic properties, that is, properties conducive to catalytic reactions such as a rich number of active sites and rapid charge migration. However, current piezoelectric (photo)catalysts struggle to combine these two aspects in the same material. Especially for the synthesis of chemicals, the surface acid–base sites of the catalyst should also be considered. Perhaps, constructing composite materials will become the main approach for the design of future piezo-(photo)catalysts.

(IV) The development of reactors. From the summary, it can be seen that the reactors used in laboratories for synthesizing chemicals through piezo-(photo)catalytic technology are quite rudimentary. Most are quartz tubes, beakers, *etc.*, which are completely inadequate for industrial production. The design and development of continuous flow industrial-grade piezo-(photo)catalytic reactors is a necessity for the future.

(V) The large-scale production of inexpensive, stable piezo-(photo)catalysts. Currently, although a considerable number of non-centrosymmetric piezo-(photo)catalysts are developed for the production of chemicals, the synthesis of many of these catalysts is complex and expensive. How to scale up the preparation of efficient and stable piezoelectric catalysts is also an urgent problem that needs to be addressed in the future.

It is expected that with the relentless efforts of researchers, more and more work will be dedicated to solving these problems, and by understanding the mechanisms better, developing more efficient piezo-(photo)catalysts, and using more advanced reactors, the efficient production of value-added chemicals will be realized.

Conflicts of interest

There are no conflicts to declare.

Acknowledgements

Notes and references

1 C. Xu, P. Ravi Anusuyadevi, C. Aymonier, R. Luque and S. Marre, *Chem. Soc. Rev.*, 2019, **48**, 3868–3902.
2 J. W. Ager and A. A. Lapkin, *Science*, 2018, **360**, 707–708.
3 G. Glenk and S. Reichelstein, *Nat. Energy*, 2019, **4**, 216–222.
4 A. F. Johnson, C. L. Dawson, M. G. Conners, C. C. Locke and S. M. Maxwell, *Science*, 2022, **376**, 361.
5 Y. Shi, Z. Zhao, D. Yang, J. Tan, X. Xin, Y. Liu and Z. Jiang, *Chem. Soc. Rev.*, 2023, **52**, 6938–6956.
6 M. Wang, B. Wang, F. Huang and Z. Lin, *Angew. Chem., Int. Ed.*, 2019, **58**, 7526–7536.
7 S. Tu, Y. Guo, Y. Zhang, C. Hu, T. Zhang, T. Ma and H. Huang, *Adv. Funct. Mater.*, 2020, **30**, 2005158.
8 X. Pan, X. Yang, M. Yu, X. Lu, H. Kang, M.-Q. Yang, Q. Qian, X. Zhao, S. Liang and Z. Bian, *Nat. Commun.*, 2023, **14**, 4183.
9 N. Meng, W. Liu, R. Jiang, Y. Zhang, S. Dunn, J. Wu and H. Yan, *Prog. Mater. Sci.*, 2023, **138**, 101161.
10 M. B. Starr and X. Wang, *Nano Energy*, 2015, **14**, 296–311.
11 F. Li, D. Lin, Z. Chen, Z. Cheng, J. Wang, C. Li, Z. Xu, Q. Huang, X. Liao, L.-Q. Chen, T. R. Shrout and S. Zhang, *Nat. Mater.*, 2018, **17**, 349–354.
12 K. Wang, C. Han, J. Li, J. Qiu, J. Sunarso and S. Liu, *Angew. Chem., Int. Ed.*, 2022, **61**, e202110429.
13 X. Zhou, B. Shen, A. Lyubartsev, J. Zhai and N. Hedin, *Nano Energy*, 2022, **96**, 107141.
14 R. Mohanty, S. Mansingh, K. Parida and K. Parida, *Mater. Horiz.*, 2022, **9**, 1332–1355.
15 C. Hu, S. Tu, N. Tian, T. Ma, Y. Zhang and H. Huang, *Angew. Chem., Int. Ed.*, 2021, **60**, 16309–16328.
16 K.-S. Hong, H. Xu, H. Konishi and X. Li, *J. Phys. Chem. Lett.*, 2010, **1**, 997–1002.
17 Z. L. Wang, *Nano Today*, 2010, **5**, 540–552.

18 Y. Zhang, H. Khanbareh, S. Dunn, C. R. Bowen, H. Gong, N. P. H. Duy and P. T. T. Phuong, *Adv. Sci.*, 2022, **9**, 2105248.

19 P. Wang, Q. Tang, L. Zhang, M. Xu, L. Sun, S. Sun, J. Zhang, S. Wang and X. Liang, *ACS Nano*, 2021, **15**, 11326–11340.

20 S. Anand, K. Thekkepat and U. V. Waghmare, *Nano Lett.*, 2016, **16**, 126–131.

21 M.-L. Xu, M. Lu, G.-Y. Qin, X.-M. Wu, T. Yu, L.-N. Zhang, K. Li, X. Cheng and Y.-Q. Lan, *Angew. Chem., Int. Ed.*, 2022, **61**, e202210700.

22 B. Bagchi, N. A. Hoque, N. Janowicz, S. Das and M. K. Tiwari, *Nano Energy*, 2020, **78**, 105339.

23 J. Ma, S. Jing, Y. Wang, X. Liu, L.-Y. Gan, C. Wang, J.-Y. Dai, X. Han and X. Zhou, *Adv. Energy Mater.*, 2022, **12**, 2200253.

24 H. Mohapatra, M. Kleiman and A. P. Esser-Kahn, *Nat. Chem.*, 2017, **9**, 135–139.

25 F. Bößl and I. Tudela, *Curr. Opin. Green Sustainable Chem.*, 2021, **32**, 100537.

26 L. Pan, S. Sun, Y. Chen, P. Wang, J. Wang, X. Zhang, J.-J. Zou and Z. L. Wang, *Adv. Energy Mater.*, 2020, **10**, 2000214.

27 C. Wang, C. Hu, F. Chen, T. Ma, Y. Zhang and H. Huang, *Nano Energy*, 2023, **107**, 108093.

28 J. Liu, W. Qi, M. Xu, T. Thomas, S. Liu and M. Yang, *Angew. Chem., Int. Ed.*, 2023, **62**, e202213927.

29 S. Chen, P. Zhu, L. Mao, W. Wu, H. Lin, D. Xu, X. Lu and J. Shi, *Adv. Mater.*, 2023, **35**, 2208256.

30 H. Sudrajat, I. Rossetti and J. C. Colmenares, *J. Mater. Chem. A*, 2023, **11**, 24566–24590.

31 R. Djellabi, M. F. Ordonez, F. Conte, E. Falletta, C. L. Bianchi and I. Rossetti, *J. Hazard. Mater.*, 2022, **421**, 126792.

32 C.-C. Jin, D.-M. Liu and L.-X. Zhang, *Small*, 2023, **19**, 2303586.

33 H. Zheng, Y. Wang, J. Liu, J. Wang, K. Yan and K. Zhu, *Appl. Catal., B*, 2024, **341**, 123335.

34 S. Xu, W. Qian, D. Zhang, X. Zhao, X. Zhang, C. Li, C. R. Bowen and Y. Yang, *Nano Energy*, 2020, **77**, 105305.

35 W. Qi, J. Liu, X. Guo, H. Guo, T. Thomas, Y. Zhu, S. Liu and M. Yang, *ACS Appl. Nano Mater.*, 2023, **6**, 2636–2645.

36 Y. Zhang, M. Xie, V. Adamaki, H. Khanbareh and C. R. Bowen, *Chem. Soc. Rev.*, 2017, **46**, 7757–7786.

37 W. Qi, H. Wang, J. Liu, T. Thomas, S. Liu and M. Yang, *Mater. Chem. Front.*, 2023, **7**, 607–627.

38 Z. Cheng, W. Qi, C. H. Pang, T. Thomas, T. Wu, S. Liu and M. Yang, *Adv. Funct. Mater.*, 2021, **31**, 2100553.

39 W. Dong, H. Xiao, Y. Jia, L. Chen, H. Geng, S. U. H. Bakhtiar, Q. Fu and Y. Guo, *Adv. Sci.*, 2022, **9**, 2105368.

40 Y.-J. Chung, C.-S. Yang, J.-T. Lee, G. H. Wu and J. M. Wu, *Adv. Energy Mater.*, 2020, **10**, 2002082.

41 M. B. Starr, J. Shi and X. Wang, *Angew. Chem., Int. Ed.*, 2012, **51**, 5962–5966.

42 Y. Wang, X. Wen, Y. Jia, M. Huang, F. Wang, X. Zhang, Y. Bai, G. Yuan and Y. Wang, *Nat. Commun.*, 2020, **11**, 1328.

43 J. Wu, W. Wang, Y. Tian, C. Song, H. Qiu and H. Xue, *Nano Energy*, 2020, **77**, 105122.

44 R. Su, H. A. Hsain, M. Wu, D. Zhang, X. Hu, Z. Wang, X. Wang, F.-T. Li, X. Chen, L. Zhu, Y. Yang, Y. Yang, X. Lou and S. J. Pennycook, *Angew. Chem., Int. Ed.*, 2019, **58**, 15076–15081.

45 Y. Huang, Y. You, M. Wu, M. Han, J. Zhang, W. Gao, D. Xie, H. Chen, H. Ou, N. Song, C. Cheng, W. Zhuang, J. Li, Z. Lei, B. Jin, Z. Zhou and M. Li, *Environ. Res.*, 2023, **229**, 115980.

46 S. F. Ahmed, M. Mofijur, N. Rafa, A. T. Chowdhury, S. Chowdhury, M. Nahrin, A. B. M. S. Islam and H. C. Ong, *Environ. Res.*, 2022, **204**, 111967.

47 M. Kozlowski and T. Yoon, *J. Org. Chem.*, 2016, **81**, 6895–6897.

48 C. Especel, G. Lafaye and F. Epron, *ChemCatChem*, 2023, **15**, e202201478.

49 C. Guo, T. Zhang, X. Deng, X. Liang, W. Guo, X. Lu and C.-M. L. Wu, *ChemSusChem*, 2019, **12**, 5126–5132.

50 N. J. Rowan and J. G. Laffey, *Sci. Total Environ.*, 2020, **725**, 138532.

51 M. Lawoko, L. Berglund and M. Johansson, *ACS Sustainable Chem. Eng.*, 2021, **9**, 5481–5485.

52 M. M. F. Hasan, L. M. Rossi, D. P. Debecker, K. C. Leonard, Z. Li, B. C. E. Makhubela, C. Zhao and A. Kleij, *ACS Sustainable Chem. Eng.*, 2021, **9**, 12427–12430.

53 R. Daiyan, I. MacGill and R. Amal, *ACS Energy Lett.*, 2020, **5**, 3843–3847.

54 P.-Z. Wang, J.-R. Chen and W.-J. Xiao, *J. Am. Chem. Soc.*, 2023, **145**, 17527–17550.

55 Y. Oh, J. O. Hwang, E.-S. Lee, M. Yoon, V.-D. Le, Y.-H. Kim, D. H. Kim and S. O. Kim, *ACS Appl. Mater. Interfaces*, 2016, **8**, 25438–25443.

56 C. Hu, F. Chen, Y. Wang, N. Tian, T. Ma, Y. Zhang and H. Huang, *Adv. Mater.*, 2021, **33**, 2101751.

57 K. Wang, D. Shao, L. Zhang, Y. Zhou, H. Wang and W. Wang, *J. Mater. Chem. A*, 2019, **7**, 20383–20389.

58 T. Xu, Z. Xia, H. Li, P. Niu, S. Wang and L. Li, *Energy Environ. Mater.*, 2023, **6**, e12306.

59 Y. Shao, C. Liu, H. Ma, J. Chen, C. Dong, D. Wang and Z. Mao, *Chem. Phys. Lett.*, 2022, **801**, 139748.

60 A. Mehtab, S. Banerjee, Y. Mao and T. Ahmad, *ACS Appl. Mater. Interfaces*, 2022, **14**, 44317–44329.

61 C. Hu, J. Hu, Z. Zhu, Y. Lu, S. Chu, T. Ma, Y. Zhang and H. Huang, *Angew. Chem., Int. Ed.*, 2022, **61**, e202212397.

62 W. Wang and S.-P. Gao, *Int. J. Hydrogen Energy*, 2022, **47**, 8761–8775.

63 C. Du, C. Bai, Y. Shui, Y. Zhao, X. Zheng, S. Guo, Q. Wang, T. Yang, S. Wang, W. Dong and L. Wang, *ACS Appl. Nano Mater.*, 2019, **2**, 879–889.

64 C. Fu, T. Wu, G. Sun, G. Yin, C. Wang, G. Ran and Q. Song, *Appl. Catal., B*, 2023, **323**, 122196.

65 L. Fang, K. Wang, C. Han, X. Li, P. Li, J. Qiu and S. Liu, *Chem. Eng. J.*, 2023, **461**, 141866.

66 K. Wang, M. Zhang, D. Li, L. Liu, Z. Shao, X. Li, H. Arandiyan and S. Liu, *Nano Energy*, 2022, **98**, 107251.

67 Y. Zhang, Y. Lin, R. Li, Z. Chen, D. Zeng, S. Chen, W. Wang, L. Zhang, W. Wang, H. Nie and G. Wang, *Chem. Eng. J.*, 2023, **465**, 143043.

68 Y. Wen, W. Liu, P. Wang, H. Che, C. Tang, B. Liu and Y. Ao, *Adv. Funct. Mater.*, 2023, **33**, 2308084.

69 J. Xu, Q. Zhang, X. Gao, P. Wang, H. Che, C. Tang and Y. Ao, *Angew. Chem., Int. Ed.*, 2023, **62**, e202307018.

70 G. Yin, C. Fu, F. Zhang, T. Wu, S. Hao, C. Wang and Q. Song, *J. Alloys Compd.*, 2023, **937**, 168382.

71 W.-J. Xu, S. Kopyl, A. Kholkin and J. Rocha, *Coord. Chem. Rev.*, 2019, **387**, 398–414.

72 Z. Wei, W.-Q. Liao, Y.-Y. Tang, P.-F. Li, P.-P. Shi, H. Cai and R.-G. Xiong, *J. Am. Chem. Soc.*, 2018, **140**, 8110–8113.

73 B. L. Green, A. T. Collins and C. M. Breeding, *Rev. Mineral. Geochem.*, 2022, **88**, 637–688.

74 B. L. Wang, J. S. Hu and L. Zheng, *Mech. Mater.*, 2023, **176**, 104415.

75 J. He, F. Gao, H. Wang, F. Liu, J. Lin, B. Wang, C. Liu, F. Huang, Z. Lin and M. Wang, *Environ. Sci.: Nano*, 2022, **9**, 1952–1960.

76 R. Das, S. Chakraborty and S. C. Peter, *ACS Energy Lett.*, 2021, **6**, 3270–3274.

77 Q. Wang, L. Ren, J. Zhang, X. Chen, C. Chen, F. Zhang, S. Wang, J. Chen and J. Wei, *Adv. Energy Mater.*, 2023, **13**, 2301543.

78 R. Yue, S. G. Ramaraj, H. Liu, D. Elamaran, V. Elamaran, V. Gupta, S. Arya, S. Verma, S. Satapathi, Y. Hayawaka and X. Liu, *J. Alloys Compd.*, 2022, **918**, 165653.

79 L. Houston, D. J. Heldebrant, E. Fox, D. A. Cullen, O. K. Farha and J. Liu, *ACS Appl. Mater. Interfaces*, 2022, **14**, 20303–20305.

80 N. Wang, R.-X. Wang, Z.-J. Li, R. Liu, H. Gao, H.-Y. Chen, R. Li, Y.-Z. Long and H.-D. Zhang, *ACS Appl. Nano Mater.*, 2023, **6**, 15063–15072.

81 Z. Pan, J. Chen, R. Yu, H. Yamamoto, Y. Rong, L. Hu, Q. Li, K. Lin, L. You, K. Zhao, L. Fan, Y. Ren, K. Kato, M. Azuma and X. Xing, *Inorg. Chem.*, 2016, **55**, 9513–9516.

82 Y. Wei, Y. Zhang, J. Miao, W. Geng and M. Long, *Appl. Surf. Sci.*, 2021, **543**, 148791.

83 C. Wang, F. Chen, C. Hu, T. Ma, Y. Zhang and H. Huang, *Chem. Eng. J.*, 2022, **431**, 133930.

84 M. A. Syzgantseva, N. F. Stepanov and O. A. Syzgantseva, *ACS Appl. Mater. Interfaces*, 2020, **12**, 17611–17619.

85 Y. Ma, B. Wang, Y. Zhong, Z. Gao, H. Song, Y. Zeng, X. Wang, F. Huang, M.-R. Li and M. Wang, *Chem. Eng. J.*, 2022, **446**, 136958.

86 X. Liao, H. Xie, B. Liao, S. Hou, Y. Yu and X. Fan, *Nano Energy*, 2022, **94**, 106890.

87 J. Cao, H. Zhou, C. Huang, Q. Wu and W. Yao, *J. Colloid Interface Sci.*, 2023, **645**, 794–805.

88 Y. Jia, K. Wang, C. Li and S. Liu, *Mater. Today Sustain.*, 2023, **22**, 100390.

89 H. Liu, S. Yu, Z. Wang and S. Xiao, *Phys. Status Solidi A*, 2021, **218**, 2100292.

90 Y. Li, Z. Li, X. Lin, H. Lv and M. Zhu, *Chem. Commun.*, 2023, **59**, 5749–5752.

91 X. Zhang and M. Z. Yates, *ACS Appl. Mater. Interfaces*, 2018, **10**, 17232–17239.

92 S. Verma and A. Yadav, *Energy Fuels*, 2023, **37**, 5712–5742.

93 R. J. Batrice and J. C. Gordon, *RSC Adv.*, 2021, **11**, 87–113.

94 V. S. Thoi and J. Y. Yang, *ACS Energy Lett.*, 2019, **4**, 2201–2204.

95 Z. Ren, F. Chen, Q. Zhao, G. Zhao, H. Li, W. Sun, H. Huang and T. Ma, *Appl. Catal., B*, 2023, **320**, 122007.

96 D. Wang, Z. Fan, G. Rao, G. Wang, Y. Liu, C. Yuan, T. Ma, D. Li, X. Tan, Z. Lu, A. Feteira, S. Liu, C. Zhou and S. Zhang, *Nano Energy*, 2020, **76**, 104944.

97 Z. Zeng, Y. Su, X. Quan, W. Choi, G. Zhang, N. Liu, B. Kim, S. Chen, H. Yu and S. Zhang, *Nano Energy*, 2020, **69**, 104409.

98 M. Taheri, S. Maaref, A. Kantzas, S. Bryant and S. Trudel, *Chem. Phys.*, 2023, **564**, 111701.

99 J. L. Collins, A. Tadich, W. Wu, L. C. Gomes, J. N. B. Rodrigues, C. Liu, J. Hellerstedt, H. Ryu, S. Tang, S.-K. Mo, S. Adam, S. A. Yang, M. S. Fuhrer and M. T. Edmonds, *Nature*, 2018, **564**, 390–394.

100 H. Kalhori, A. H. Youssef, A. Ruediger and A. Pignolet, *J. Environ. Chem. Eng.*, 2022, **10**, 108571.

101 J. Wu, *J. Appl. Phys.*, 2020, **127**, 190901.

102 P. T. T. Phuong, D.-V. N. Vo, N. P. H. Duy, H. Pearce, Z. M. Tsikriteas, E. Roake, C. Bowen and H. Khanbareh, *Nano Energy*, 2022, **95**, 107032.

103 J. Ma, X. Xiong, D. Wu, Y. Wang, C. Ban, Y. Feng, J. Meng, X. Gao, J.-Y. Dai, G. Han, L.-Y. Gan and X. Zhou, *Adv. Mater.*, 2023, **35**, 2300027.

104 M. Ran, H. Xu, Y. Bao, Y. Zhang, J. Zhang and M. Xing, *Angew. Chem., Int. Ed.*, 2023, **62**, e202303728.

105 W. Tian, N. Li, D. Chen, Q. Xu, H. Li, C. Yan and J. Lu, *Angew. Chem., Int. Ed.*, 2023, **62**, e202306964.

106 J. Ma, D. Wu, Y. Feng, C. Ban, L. Xia, L. Ruan, J. Guan, Y. Wang, J. Meng, J.-Y. Dai, L.-Y. Gan and X. Zhou, *Nano Energy*, 2023, **115**, 108719.

107 L. Mennel, M. Paur and T. Mueller, *APL Photonics*, 2018, **4**, 034404.

108 J. Furstoss, P. Hirel, P. Carrez and P. Cordier, *Am. Mineral.*, 2022, **107**, 2034–2043.

109 G. O. Sigge, T. J. Britz, P. C. Fourie, C. A. Barnardt and R. Strydom, *Water Sci. Technol.*, 2002, **45**, 329–334.

110 W. da Silva Freitas, A. D'Epifanio and B. Mecheri, *J. CO$_2$ Util.*, 2021, **50**, 101579.

111 Q. Qian and B. Han, *Natl. Sci. Rev.*, 2023, **10**, nwad160.

112 S. W. Boettcher, *ACS Energy Lett.*, 2020, **5**, 70–71.

113 F. Peng, J. Lin, H. Li, Z. Liu, Q. Su, Z. Wu, Y. Xiao, H. Yu, M. Zhang, C. Wu, W. Wang and C. Lu, *Nano Energy*, 2022, **95**, 107020.

114 X. Ning, D. Jia, S. Li, M. F. Khan and A. Hao, *Ceram. Int.*, 2023, **49**, 21658–21666.

115 L. Chen, X. Dai, X. Li, J. Wang, H. Chen, X. Hu, H. Lin, Y. He, Y. Wu and M. Fan, *J. Mater. Chem. A*, 2021, **9**, 13344–13354.

116 P. Peng, P. Chen, C. Schiappacasse, N. Zhou, E. Anderson, D. Chen, J. Liu, Y. Cheng, R. Hatzenbeller, M. Addy,

Y. Zhang, Y. Liu and R. Ruan, *J. Cleaner Prod.*, 2018, **177**, 597–609.

117 S. D. Minteer, P. Christopher and S. Linic, *ACS Energy Lett.*, 2019, **4**, 163–166.

118 W. Sun, Y. Zheng and J. Zhu, *Mater. Today Sustain.*, 2023, **23**, 100465.

119 M. G. Rinaudo, M. K. López González, L. E. Cadús and M. R. Morales, *J. Phys. Chem. Solids*, 2023, **183**, 111661.

120 J. Twilton, C. Le, P. Zhang, M. H. Shaw, R. W. Evans and D. W. C. MacMillan, *Nat. Rev. Chem.*, 2017, **1**, 0052.

121 H. Xia and Z. Wang, *Science*, 2019, **366**, 1451–1452.

122 Q. Zhang, Y. Jia, W. Wu, C. Pei, G. Zhu, Z. Wu, L. Zhang, W. Fan and Z. Wu, *Nano Energy*, 2023, **113**, 108507.

123 L. A. Rishina, Y. V. Kissin, S. C. Gagieva and S. S. Lalayan, *Russ. J. Phys. Chem. B*, 2019, **13**, 789–802.

124 S. Akbulatov, Y. Tian, Z. Huang, T. J. Kucharski, Q.-Z. Yang and R. Boulatov, *Science*, 2017, **357**, 299–303.

125 K. Kubota, Y. Pang, A. Miura and H. Ito, *Science*, 2019, **366**, 1500–1504.

126 Y. Pang, J. W. Lee, K. Kubota and H. Ito, *Angew. Chem., Int. Ed.*, 2020, **59**, 22570–22576.

127 X. Wang, X. Zhang, L. Xue, Q. Wang, F. You, L. Dai, J. Wu, S. Kramer and Z. Lian, *Angew. Chem., Int. Ed.*, 2023, **62**, e202307054.

128 Y. Wang, Z. Zhang, L. Deng, T. Lao, Z. Su, Y. Yu and H. Cao, *Org. Lett.*, 2021, **23**, 7171–7176.

129 M. Huang, L. Deng, T. Lao, Z. Zhang, Z. Su, Y. Yu and H. Cao, *J. Org. Chem.*, 2022, **87**, 3265–3275.

130 M. D. Nothling, J. E. Daniels, Y. Vo, I. Johan and M. H. Stenzel, *Angew. Chem., Int. Ed.*, 2023, **62**, e202218955.

131 H. Lv, X. Xu, J. Li, X. Huang, G. Fang and L. Zheng, *Angew. Chem., Int. Ed.*, 2022, **61**, e202206420.

132 J. Yoon, J. Kim, F. Tieves, W. Zhang, M. Alcalde, F. Hollmann and C. B. Park, *ACS Catal.*, 2020, **10**, 5236–5242.

133 F. Liu, L. N. Chen, A. M. Chen, Z. P. Ye, Z. W. Wang, Z. L. Liu, X. C. He, S. H. Li and P. J. Xia, *Adv. Synth. Catal.*, 2022, **364**, 1080–1084.

134 L. Song, T. Zhang, S. Zhang, J. Wei and E. Chen, *ACS Sustainable Chem. Eng.*, 2022, **10**, 5129–5137.

135 Z. Chen, H. Zhou, F. Kong and M. Wang, *Appl. Catal., B*, 2022, **309**, 121281.

136 Y. Zhou, H. Wang, X. Liu, S. Qiao, D. Shao, J. Zhou, L. Zhang and W. Wang, *Nano Energy*, 2021, **79**, 105449.

137 V. Navakoteswara Rao, T. J. Malu, K. K. Cheralathan, M. Sakar, S. Pitchaimuthu, V. Rodríguez-González, M. Mamatha Kumari and M. V. Shankar, *J. Environ. Manage.*, 2021, **284**, 111983.

138 X. Zhang, Y. Wang, K. Chang, S. Yang, H. Liu, Q. Chen, Z. Xie and Q. Kuang, *Appl. Catal., B*, 2023, **320**, 121961.

139 J. Yuan, X. Huang, L. Zhang, F. Gao, R. Lei, C. Jiang, W. Feng and P. Liu, *Appl. Catal., B*, 2020, **278**, 119291.

140 L. Jing, Y. Xu, M. Xie, Z. Li, C. Wu, H. Zhao, J. Wang, H. Wang, Y. Yan, N. Zhong, H. Li and J. Hu, *Nano Energy*, 2023, **112**, 108508.

141 J. He, X. Wang, S. Lan, H. Tao, X. Luo, Y. Zhou and M. Zhu, *Appl. Catal., B*, 2022, **317**, 121747.

142 J. He, X. Wang, S. Lan, H. Tao, X. Luo, Y. Zhou and M. Zhu, *Appl. Catal., B*, 2022, 317.

143 H. Deng, C. Qin, K. Pei, G. Wu, M. Wang, H. Ni and P. Ye, *Mater. Chem. Phys.*, 2021, **270**, 124796.

144 Y. Wang, X. Li, Y. Chen, Y. Li, Z. Liu, C. Fang, T. Wu, H. Niu, Y. Li, W. Sun, W. Tang, W. Xia, K. Song, H. Liu and W. Zhou, *Adv. Mater.*, 2023, **35**, 2305257.

145 J. Yuan, W. Feng, Y. Zhang, J. Xiao, X. Zhang, Y. Wu, W. Ni, H. Huang and W. Dai, *Adv. Mater.*, 2024, **36**, 2303845.

146 X. Zhou, F. Yan, A. Lyubartsev, B. Shen, J. Zhai, J. C. Conesa and N. Hedin, *Adv. Sci.*, 2022, **9**, 2105792.

147 X. Wang, J. Jiang, L. Yang, Q. An, Q. Xu, Y. Yang and H. Guo, *Appl. Catal., B*, 2024, **340**, 123177.

148 G. Yang, S. Wang, Y. Wu, H. Zhou, W. Zhao, S. Zhong, L. Liu and S. Bai, *ACS Appl. Mater. Interfaces*, 2023, **15**, 14228–14239.

149 Q. Xu, L. Wang, X. Sheng, Y. Yang, C. Zhang, L. Duan and H. Guo, *Appl. Catal., B*, 2023, **338**, 123058.

150 L. Zhang, K. Wang, Y. Jia, L. Fang, C. Han, J. Li, Z. Shao, X. Li, J. Qiu and S. Liu, *Adv. Funct. Mater.*, 2022, **32**, 2205121.

151 W. Qi, Z. Cheng, S. Liu and M. Yang, *Catal. Sci. Technol.*, 2023, **13**, 6864–6877.

152 M. Song, S. Yang, H. Peng, T. Zhao, F. Liu, P. Chen and S.-F. Yin, *Nano Energy*, 2023, **116**, 108784.

153 H.-T. Vuong, D.-V. Nguyen, P. P. Ly, P. D. M. Phan, T. D. Nguyen, D. D. Tran, P. T. Mai and N. H. Hieu, *ACS Appl. Nano Mater.*, 2023, **6**, 664–676.

154 D. D. Tran, H.-T. Vuong, D.-V. Nguyen, P. P. Ly, P. D. Minh Phan, V. H. Khoi, P. T. Mai and N. H. Hieu, *Nanoscale Adv.*, 2023, **5**, 2327–2340.

155 H. Zhang, Z. Xia, P. Niu, X. Zhi, R. Dai, S. Chen, S. Wang and L. Li, *Catal. Sci. Technol.*, 2022, **12**, 5372–5378.

156 P. Wang, S. Fan, X. Li, J. Duan and D. Zhang, *ACS Catal.*, 2023, **13**, 9515–9523.

157 Z. Li, Y. Zhou, Y. Zhou, K. Wang, Y. Yun, S. Chen, W. Jiao, L. Chen, B. Zou and M. Zhu, *Nat. Commun.*, 2023, **14**, 5742.

158 C. Fu, M. Zhao, X. Chen, G. Sun, C. Wang and Q. Song, *Appl. Catal., B*, 2023, **332**, 122752.

159 P. D. M. Phan, D.-V. Nguyen, N. H. Anh, H. P. Toan, P. P. Ly, D.-P. Bui, S. H. Hur, T. D. T. Ung, D. D. Bich and H.-T. Vuong, *ACS Appl. Nano Mater.*, 2023, **6**, 16702–16715.

160 S. Wang, L. Wang and W. Huang, *J. Mater. Chem. A*, 2020, **8**, 24307–24352.

161 Z.-F. Huang, L. Pan, J.-J. Zou, X. Zhang and L. Wang, *Nanoscale*, 2014, **6**, 14044–14063.

162 S. Tu, Y. Wang, H. Huang, J. Zhang, H. Li, J. Sun, T. Chen and Y. Zhang, *Chem. Eng. J.*, 2023, **465**, 142777.

163 L. Chen, W. Zhang, J. Wang, X. Li, Y. Li, X. Hu, L. Zhao, Y. Wu and Y. He, *Green Energy Environ.*, 2023, **8**, 283–295.

164 X. Deng, P. Chen, R. Cui, W. Huang, Y. Wu, X. Wang and C. Deng, *Appl. Catal., B*, 2023, **339**, 123148.

165 P. Wang, X. Li, S. Fan, Z. Yin, L. Wang, M. O. Tadé and S. Liu, *Nano Energy*, 2021, **83**, 105831.

166 M. Chen, J. Bi, X. Huang, J. Wang, T. Wang, Z. Wang and H. Hao, *Nanoscale*, 2021, **13**, 13786–13794.

167 V. Kyriakou, I. Garagounis, A. Vourros, E. Vasileiou and M. Stoukides, *Joule*, 2020, **4**, 142–158.

168 S. Lin, Q. Wang, H. Huang and Y. Zhang, *Small*, 2022, **18**, 2200914.

169 P. Wang, S. Fan, X. Li, J. Wang, Z. Liu, C. Bai, M. O. Tadé and S. Liu, *Nano Energy*, 2021, **89**, 106349.

170 A. K. Kole, S. Karmakar, A. Pramanik and P. Kumbhakar, *Nanotechnology*, 2023, **34**, 282001.

171 Y. Tong, Y. Hou, Z. Zhang, L. Yan, X. Chen, H. Zhang, X. Wang and Y. Li, *Appl. Catal., A*, 2023, **665**, 119387.

172 T. Heliso Dolla, T. Matthews, N. Wendy Maxakato, P. Ndungu and T. Montini, *J. Electroanal. Chem.*, 2023, **928**, 117049.